

THE SECOND CALTECH-JODRELL BANK VLBI SURVEY. II. OBSERVATIONS OF 102 OF 193 SOURCES

D. R. HENSTOCK, I. W. A. BROWNE, AND P. N. WILKINSON

University of Manchester, Nuffield Radio Astronomy Laboratories, Jodrell Bank, Macclesfield, Cheshire SK11 9DL, UK

AND

G. B. TAYLOR, R. C. VERMEULEN, T. J. PEARSON, AND A. C. S. READHEAD

California Institute of Technology, Owens Valley Radio Observatory, 105-24, Pasadena, CA 91125

Received 1994 November 21; accepted 1995 February 1

ABSTRACT

This is the second of two papers presenting the Second Caltech–Jodrell Bank VLBI survey (CJ2). The CJ2 sample consists of 193 flat- and gigahertz-peaked-spectrum sources selected at 4850 MHz. In this paper we present images of the remaining 102 sources with a resolution of ~ 1 mas, obtained using VLBI snapshot observations at 4992 MHz with a global array. We also present integrated radio spectra for the entire CJ2 sample.

Subject headings: quasars: general — radio continuum: galaxies — surveys

1. INTRODUCTION

The second Caltech–Jodrell Bank VLBI survey (CJ2) is a Mark II snapshot VLBI survey of 193 flat- and gigahertz-peaked-spectrum radio sources, observed at a frequency of 4992 MHz. The main aims of CJ2 are to extend the morphological classification started by the Pearson & Readhead survey (Pearson & Readhead 1988, hereafter PR), and first Caltech–Jodrell Bank VLBI survey (Polatidis et al. 1995; Thakkar et al. 1995; Xu et al. 1995; hereafter CJ1) and to address three cosmological goals. These goals are (1) to place significant limits on the mass in 10^6 – $10^9 M_\odot$ condensed objects by searching for gravitational lenses with a separation of 1–200 mas, (2) to look for evidence of cosmological evolution in the proper motions of superluminal sources and place limits on q_0 , and (3) to explore the possibility of using the angular diameter-redshift diagram for compact objects to constrain q_0 .

In the first paper in this series (Taylor et al. 1994), we defined the CJ2 sample. We also reported on the first three observing sessions and presented VLBI images of 91 sources. We showed that the images, including those presented in this paper, are predominantly limited by thermal noise and not by dynamic range. Hence CJ2 is an excellent, uniform sample of VLBI images, ideal for the statistical tests which are the aims of the survey.

In this paper we present the second half of the results of the CJ2 survey. In § 2 we describe the fourth and final observing session, and in § 3 we present VLBI images of the remaining 102 sources. In § 4 we present integrated radio spectra, compiled from the literature, for all 193 sources in the CJ2 sample.

A redshift program of observations of CJ2 sources which have no measured redshift is well underway (Vermeulen & Taylor 1995); $\sim 70\%$ of CJ2 sources now have a measured redshift.

2. OBSERVATIONS

The observations presented in this paper were made from 1993 June 9 to June 16. Thirteen telescopes from the European VLBI Network (EVN), the US National Radio Astronomy

Observatory's Very Large Baseline Array¹ (VLBA; Napier et al. 1994), and the VLA¹ participated successfully. Their characteristics are listed in Table 1. The observing frequency was 4992 MHz, and left-circular polarization was recorded using the Mark II system with 2 MHz bandwidth.

The VLBI snapshot technique was used, as in the previous sessions detailed in Paper I. Each source was observed for three to five scans of 20 minutes duration, the scans being approximately equally spaced over a wide range in hour angle. The sources observed in this session were mainly of low declination ($\delta \sim 35^\circ$ – 50°), and since fewer telescopes observed successfully than in previous sessions, the u - v coverage was generally poorer than before. Figure 1 shows the typical u - v coverage for this session.

The data reduction procedure was identical to that given in Paper I, so only a brief outline will be given here. The data were correlated with the JPL/Caltech Block II correlator with clock offsets being monitored using strong calibrator sources. The data were then fringe-fitted using the AIPS task FRING, with a solution interval of ~ 7 minutes. Effelsberg was used as the reference telescope wherever possible; otherwise, the Hancock VLBA antenna was used. The amplitude calibration for each antenna, determined using measurements of antenna gain and system temperature, was adjusted by imaging strong calibrator sources and by examining the u - v crossing points. The relative amplitude calibration is accurate to $\sim 2\%$ rms, and the absolute flux calibration is accurate to better than 10%. The data were phase self-calibrated to a point-source model with a 10 s solution interval and then coherently averaged to 1 minute. Finally, the data were imaged with DIFMAP (Shepherd, Pearson, & Taylor 1994) using cycles of deconvolution and self-calibration.

3. RESULTS

In Figure 2 we present the naturally weighted images for the 102 CJ2 sources. While the lowest contour (3σ) may be

¹ The National Radio Astronomy Observatory is operated by Associated Universities, Inc., under cooperative agreement with the National Science Foundation.

TABLE 1
TELESCOPE CHARACTERISTICS

Telescope	Code	Location	Diam (m)	T_{sys} (K)	T_{sys} (Jy)	Sensitivity (K/Jy)
(1)	(2)	(3)	(4)	(5)	(6)	(7)
Jodrell MKII	J2	Jodrell Bank, UK	26	45	375	0.12
Effelsberg	B	Germany	100	58	39	1.5
Onsala	S	Sweden	26	58	983	0.059
WSRT	W	Netherlands	5×25	64	128	0.5
Medicina	L	Bologna, Italy	32	44	275	0.16
Noto	N	Noto, Italy	32	30	183	0.164
Simeiz	U	Crimea, Ukraine	22	103	3433	0.030
VLA ^a	Y	New Mexico, USA	25	57	491	0.116
VLBA_BR	BR	Brewster WA, USA	25	33	282	0.117
VLBA_HN	HN	Hancock NH, USA	25	38	309	0.123
VLBA_NL	NL	North Liberty IA, USA	25	39	390	0.100
VLBA_OV	OV	Owens Valley CA, USA	25	38	302	0.126
VLBA_PT	PT	Pie Town NM, USA	25	45	308	0.146

NOTES.—Cols. (1)–(3): The name, the code used, and the location of each telescope. Affiliations: B, Max-Planck-Institut für Radioastronomie; S, Onsala Space Observatory; W, Westerbork Synthesis Radio Telescope, NFRA; J2, Nuffield Radio Astronomy Laboratories; U, Space Research Institute, Moscow; L, N, Istituto di Radioastronomia; BR, HN, NL, OV, PT, National Radio Astronomy Observatory VLBA; Y, National Radio Astronomy Observatory VLA. Col. (4): The diameter of each telescope (in meters). Cols. (5)–(7): The system temperature in kelvins and in janskys and the sensitivity in kelvins per jansky of each telescope.

^a The VLA was used in single antenna mode.

affected by residual systematic phase and amplitude errors, the second contour is reliable. The typical dynamic range, estimated as the ratio of the peak intensity to the rms in a blank area of sky, is $\sim 500:1$, the same as that for the first three sessions. Fringe-fitting and mapping proved difficult for only one source, 1545+497, which was barely detected on the shortest baselines. Any derived parameters for this source must be interpreted with caution. Another source, 0256+424, was initially weak because the original position given by Patnaik et al.

(1992) and reproduced in Table 1 of Paper I was incorrect. This source was recorrelated at the correct position of $\alpha(J2000) = 02^{\circ}59^m37\rlap{.}^s6753$, $\delta(J2000) = 42^{\circ}35'49\rlap{.}''9079$.

Tapered images are shown in cases where they reveal additional information. These were produced by using a Gaussian taper falling to 50% at $70 \text{ M}\lambda$ on the naturally weighted self-calibrated data. All tapered images were restored with a circular 3 mas beam. The beam dimensions, rms, peak intensity, and lowest contour level (at 3σ) for both the naturally weighted and tapered maps are shown in Table 2.

Model fitting was performed on the self-calibrated amplitudes and phases of each source in order to extract quantitative information, with up to four Gaussian components being fitted to each source. Model fitting was successful (total agreement factor < 1.2) for all 102 sources, and the model components are listed for each source in Table 3. The average total agreement factor is 1.004, slightly better than the value of 1.045 obtained for the previous three sessions. A description of the agreement factors is given in the Appendix.

4. SPECTRA

Integrated radio spectra for the entire CJ2 sample, covering the frequency range 151 MHz to 90 GHz, are given in Figure 3. These were compiled from various flux density catalogs in the literature, which are listed in Table 4. All the flux densities are on the absolute scale defined by Laing & Peacock (1980, hereafter LP),² and where necessary the original flux densities were converted to this scale, using correction factors that had already been determined by previous workers.

² The LP scale is identical to that of Baars et al. (1977) above 408 MHz (Riley 1988), and we have taken it to be identical above 327 MHz. At lower frequencies (178 MHz and below) the LP scale follows that of Roger, Bridle, & Costain (1973). Note that at 151 MHz the Baars et al. scale is ~ 0.95 times the LP scale.

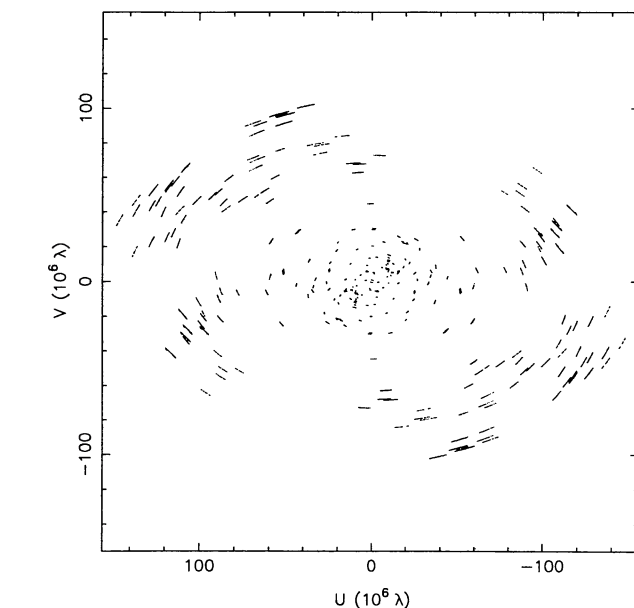


FIG. 1.—Typical u - v coverage for a source (1321+410) observed in the 1993 June session. The pattern is the result of three observations of 20 minutes each spaced over a wide range in hour angle.

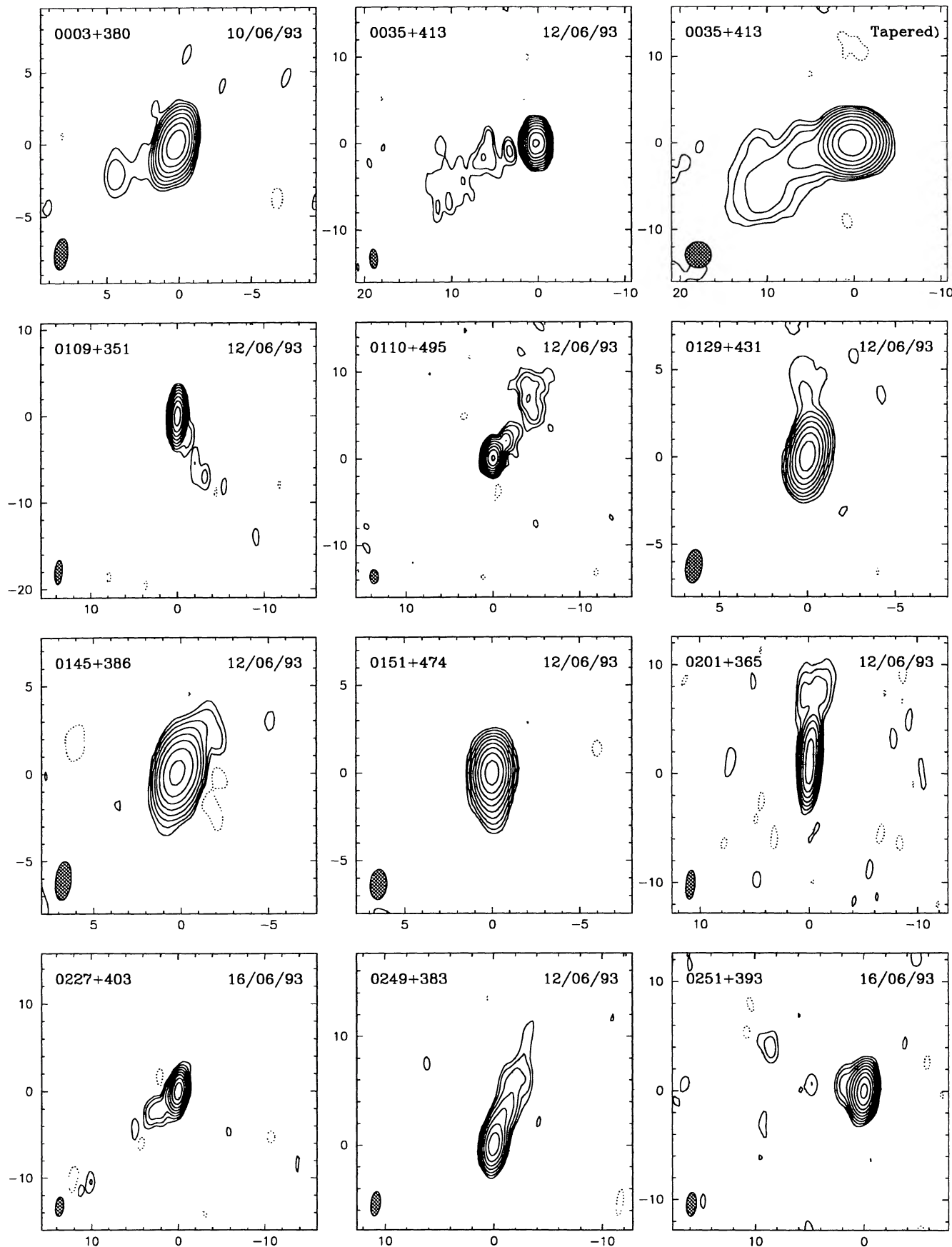


FIG. 2.—The 6 cm VLBI images for 102 sources in the CJ2 sample. Maps in which the epoch of observation is given in the upper right-hand corner are naturally weighted images, while those which are “tapered” have been weighted by a Gaussian taper and restored with a 3 mas beam as described in the text. The FWHM contour of the Gaussian beam is given in the lower left-hand corner and is listed in Table 2, along with the rms, peak intensity, and lowest contour level at 3σ . Contours are logarithmic at $-3\sigma, 3\sigma, 6\sigma, 12\sigma$, etc. Negative contours are shown as dashed lines. FITS images corresponding to the maps presented in Fig. 2 are published in the AAS CD-ROM Series, Vol. 4.

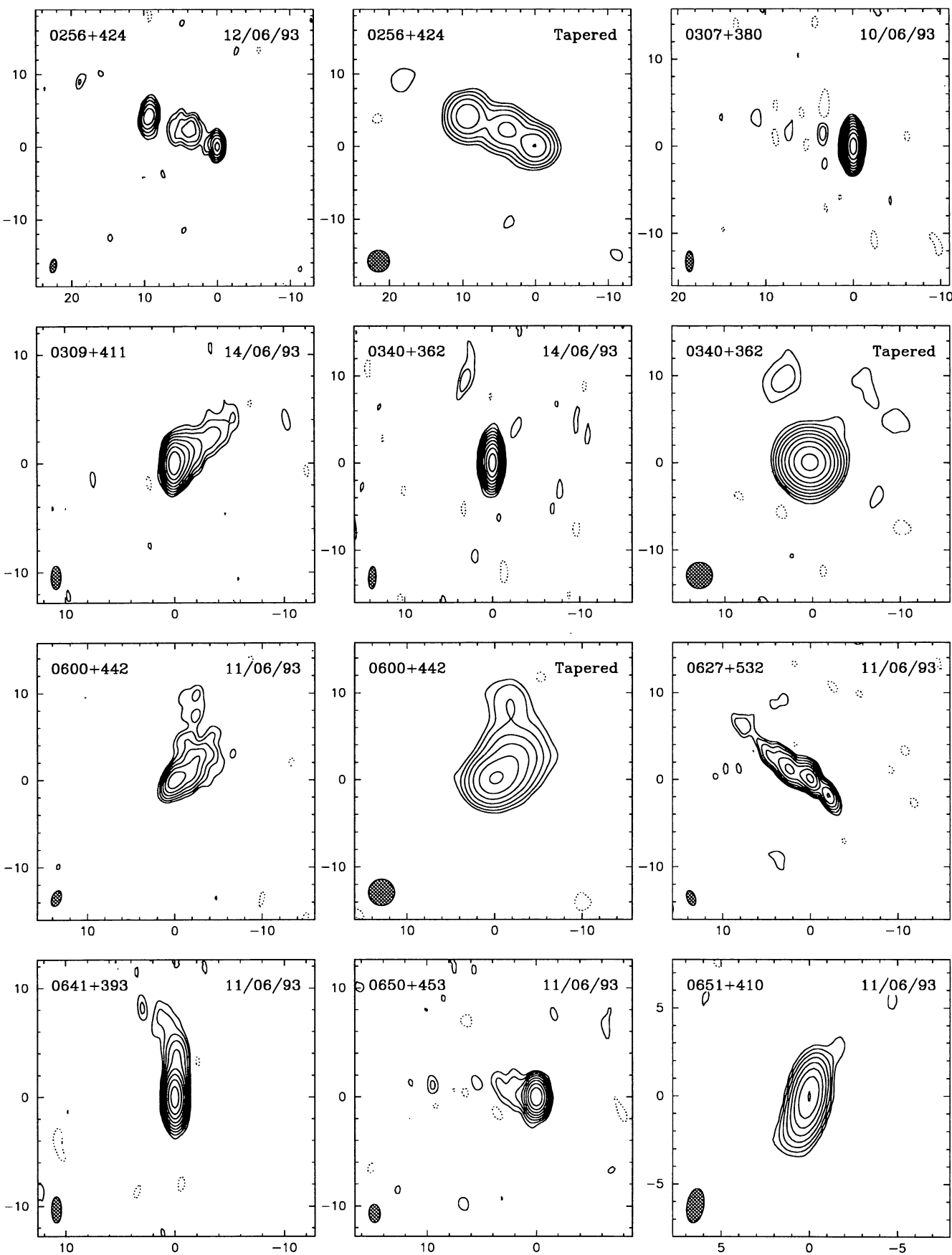


FIG. 2—Continued

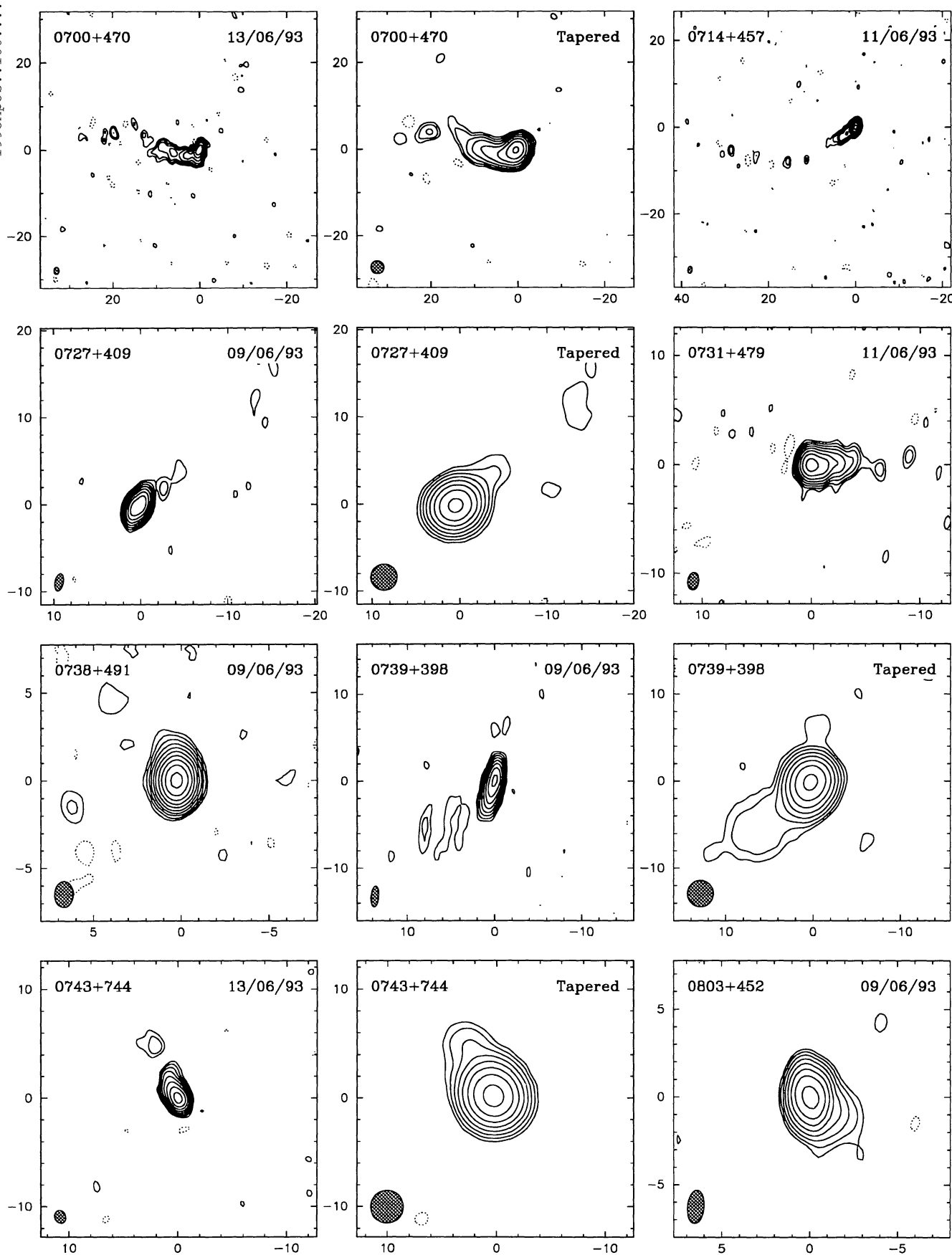


FIG. 2—Continued

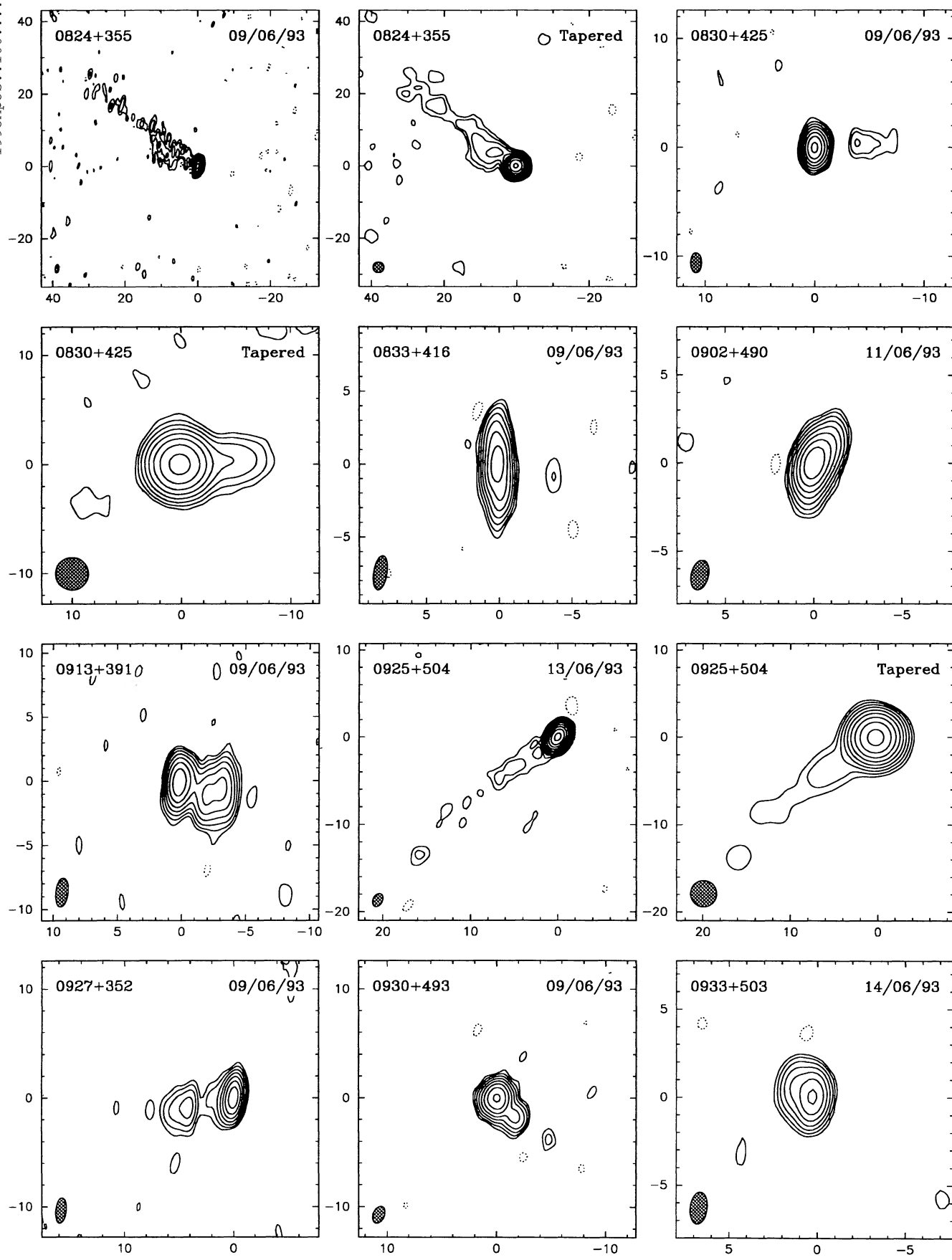


FIG. 2—Continued

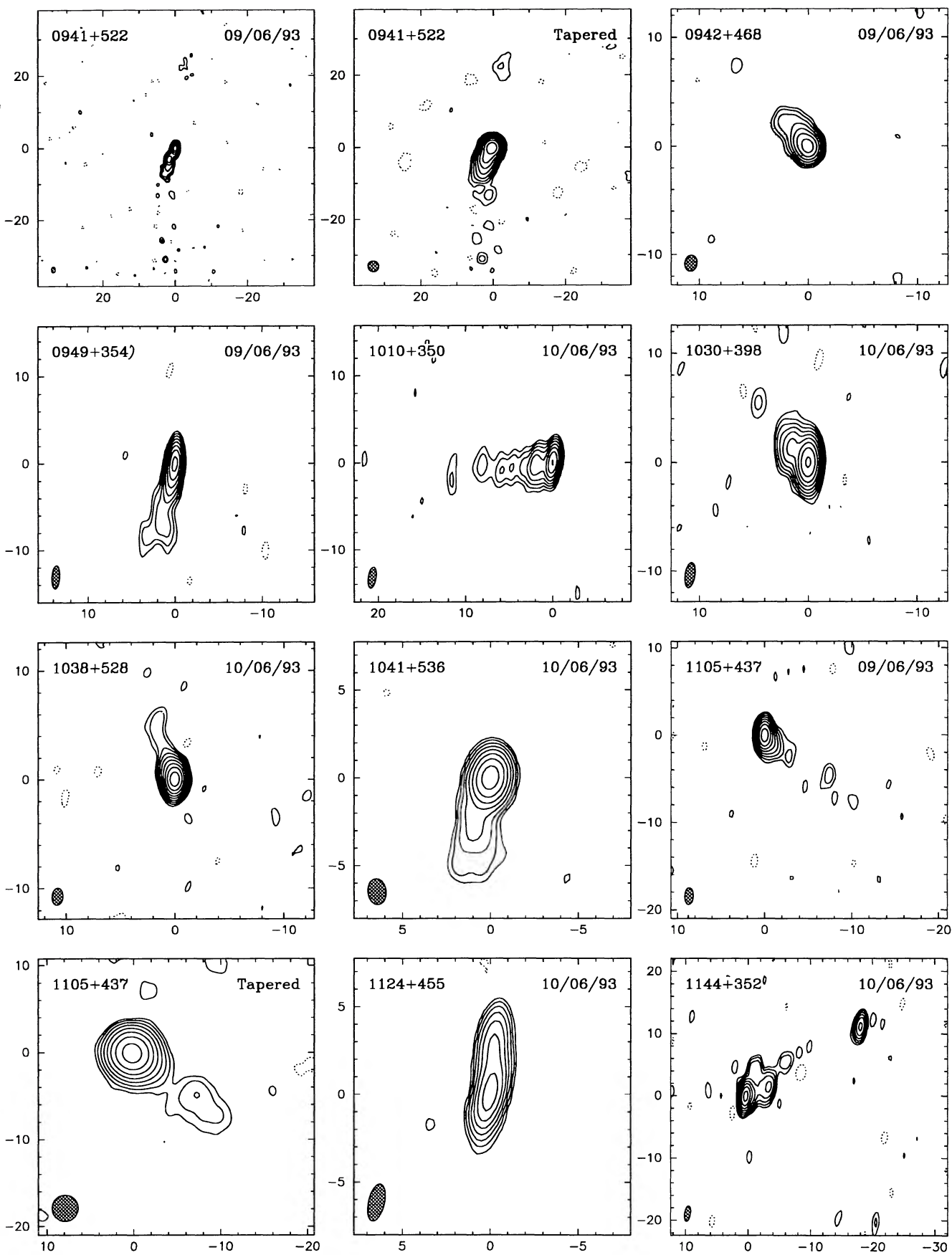


FIG. 2—Continued

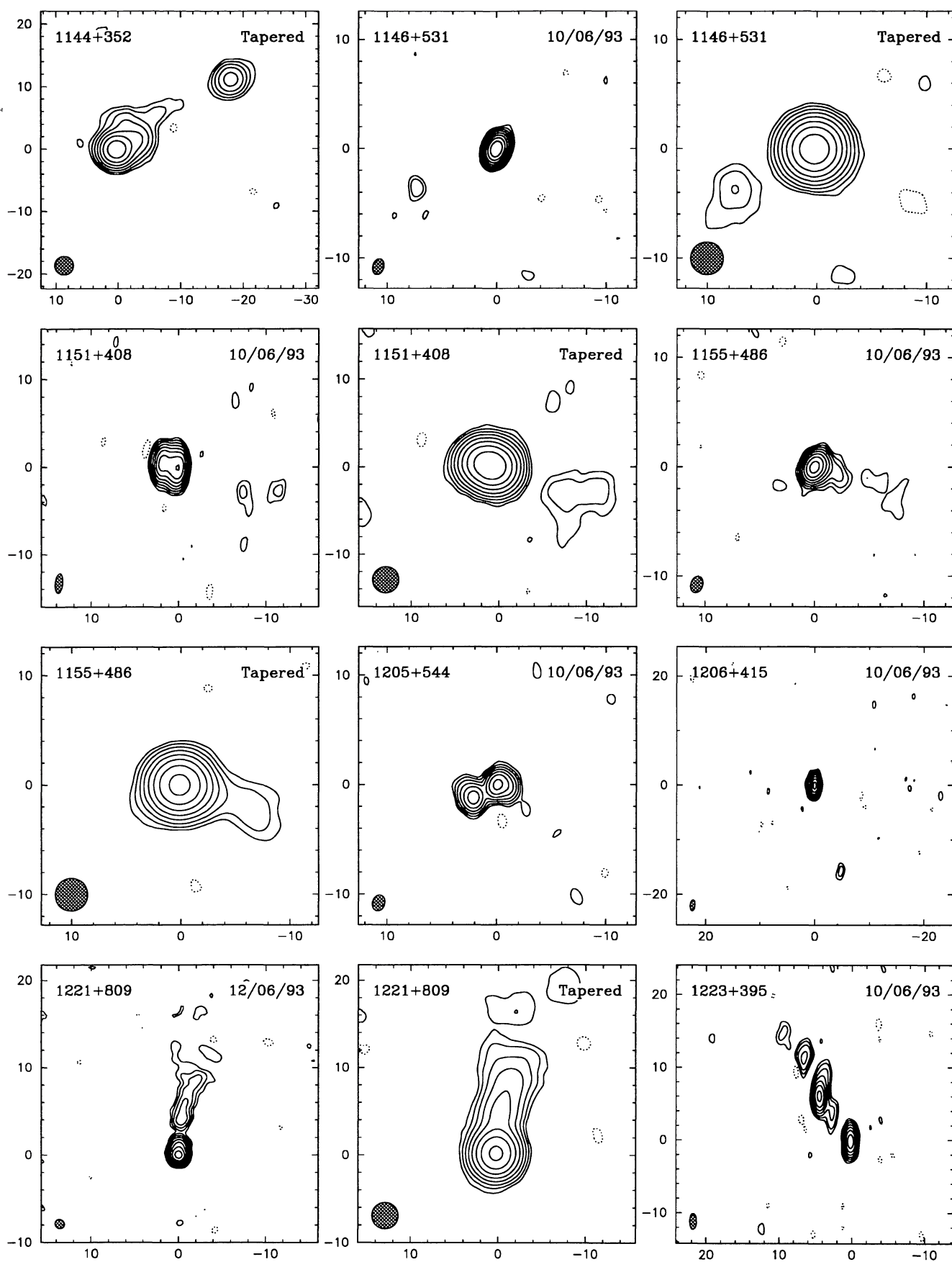


FIG. 2—Continued

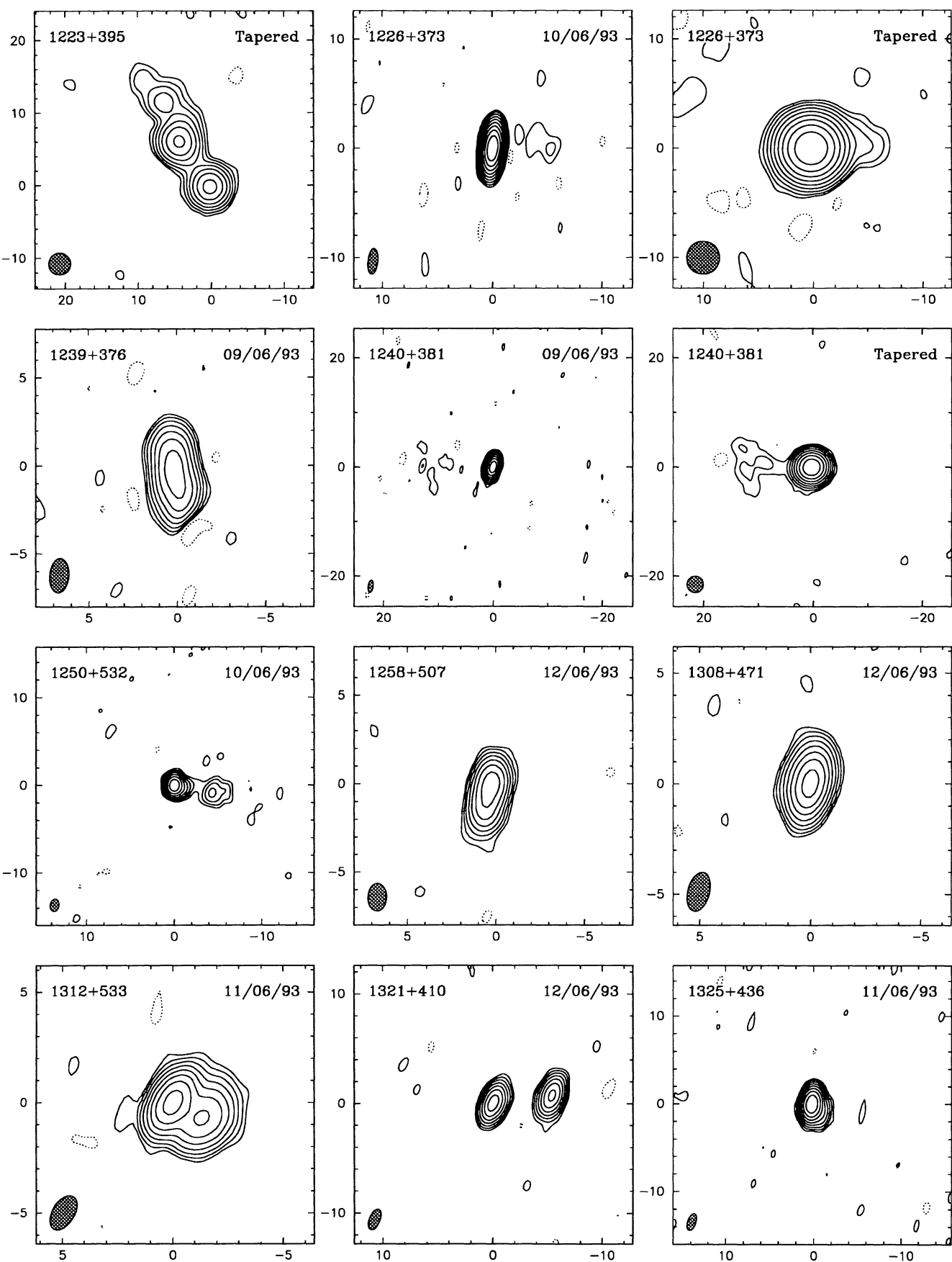


FIG. 2—Continued

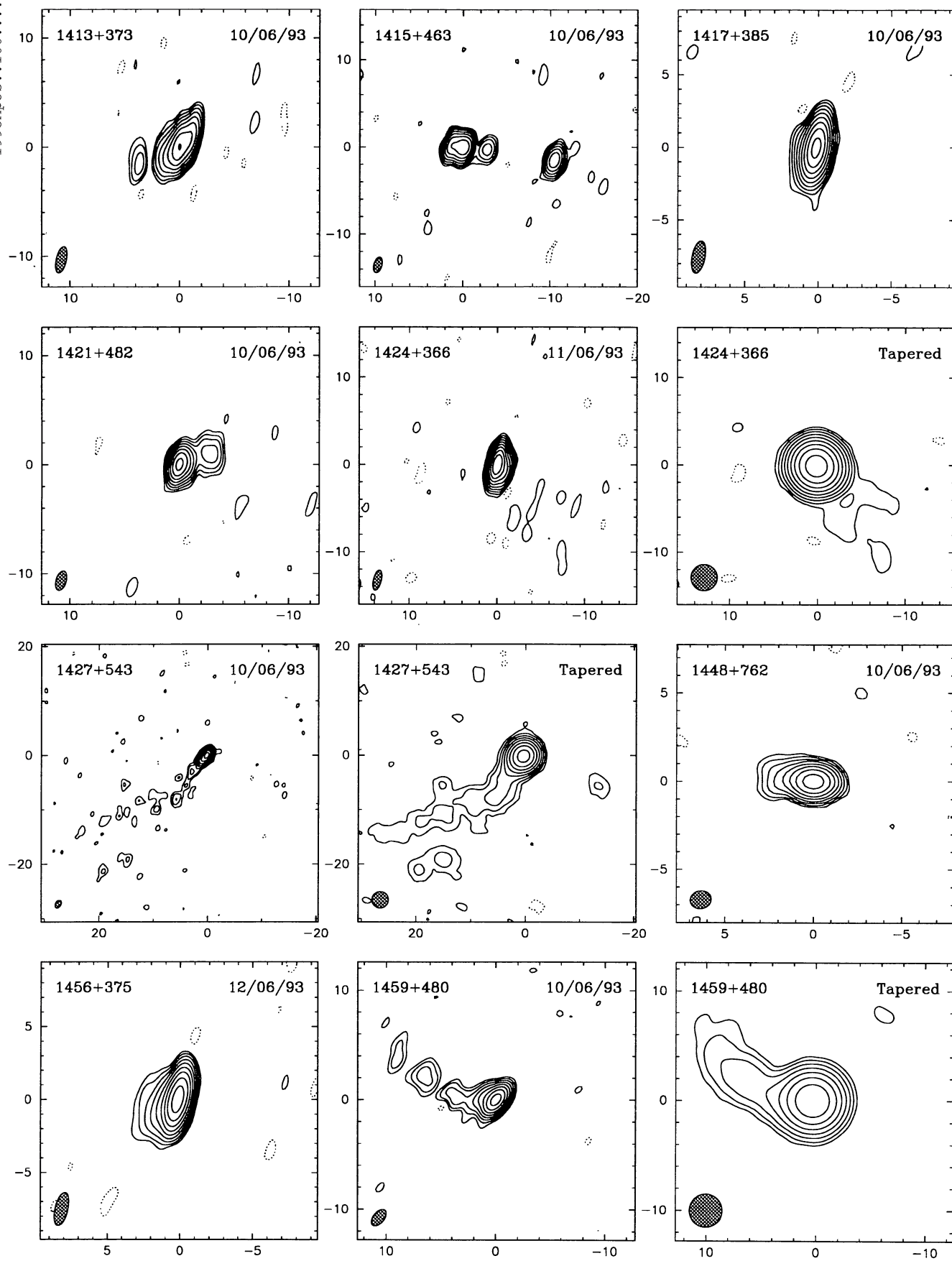


FIG. 2—Continued

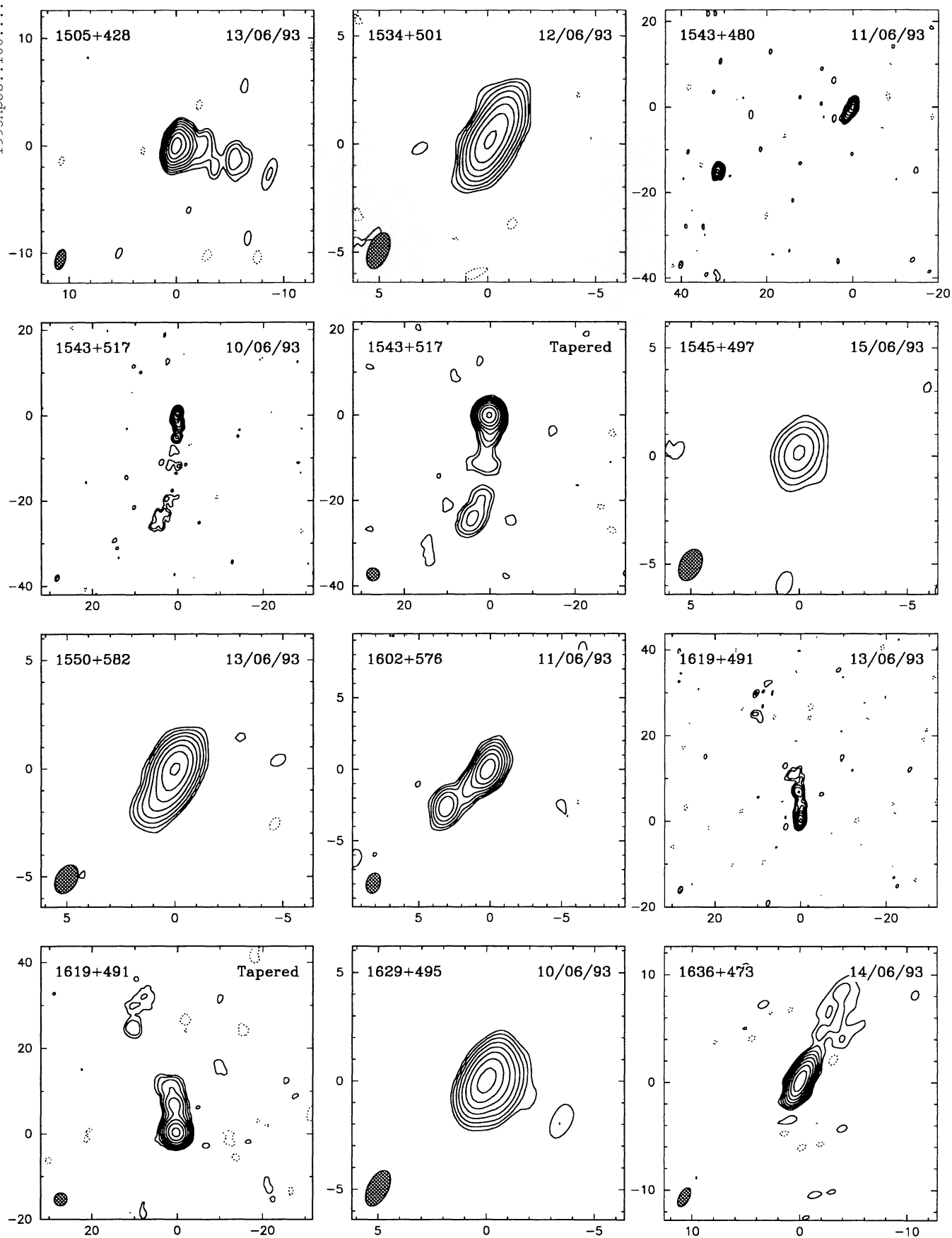


FIG. 2—Continued

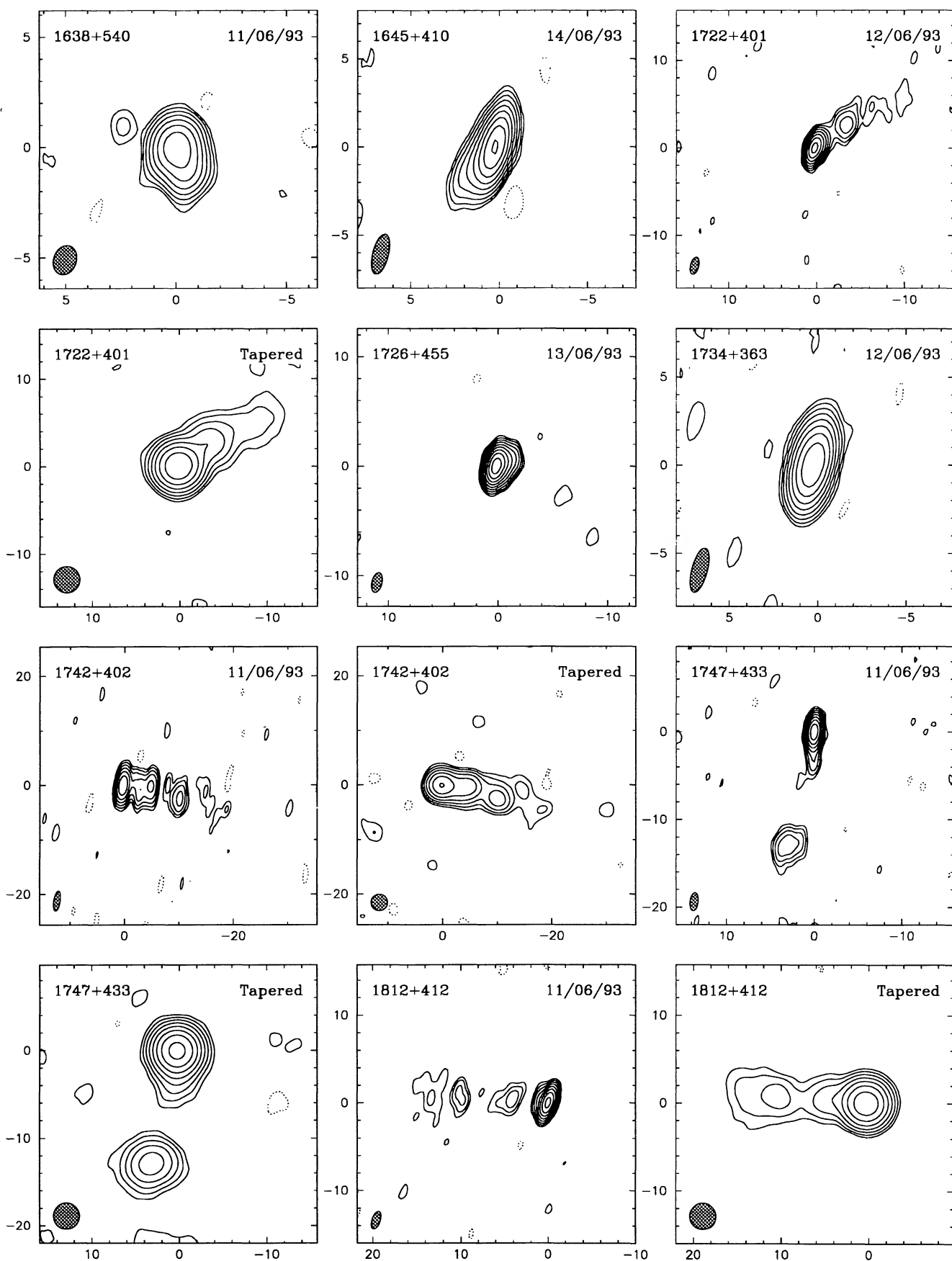


FIG. 2—Continued

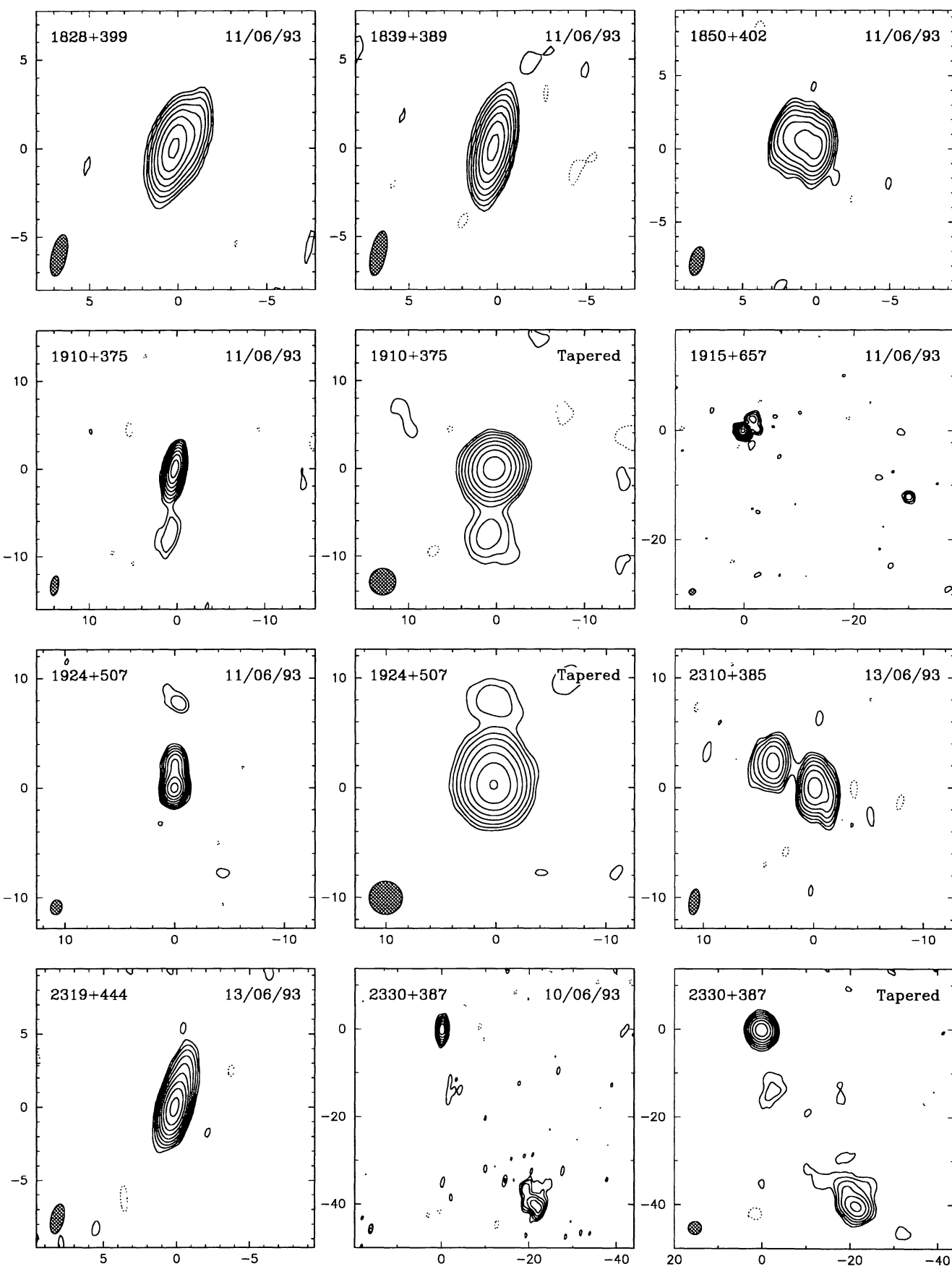


FIG. 2—Continued

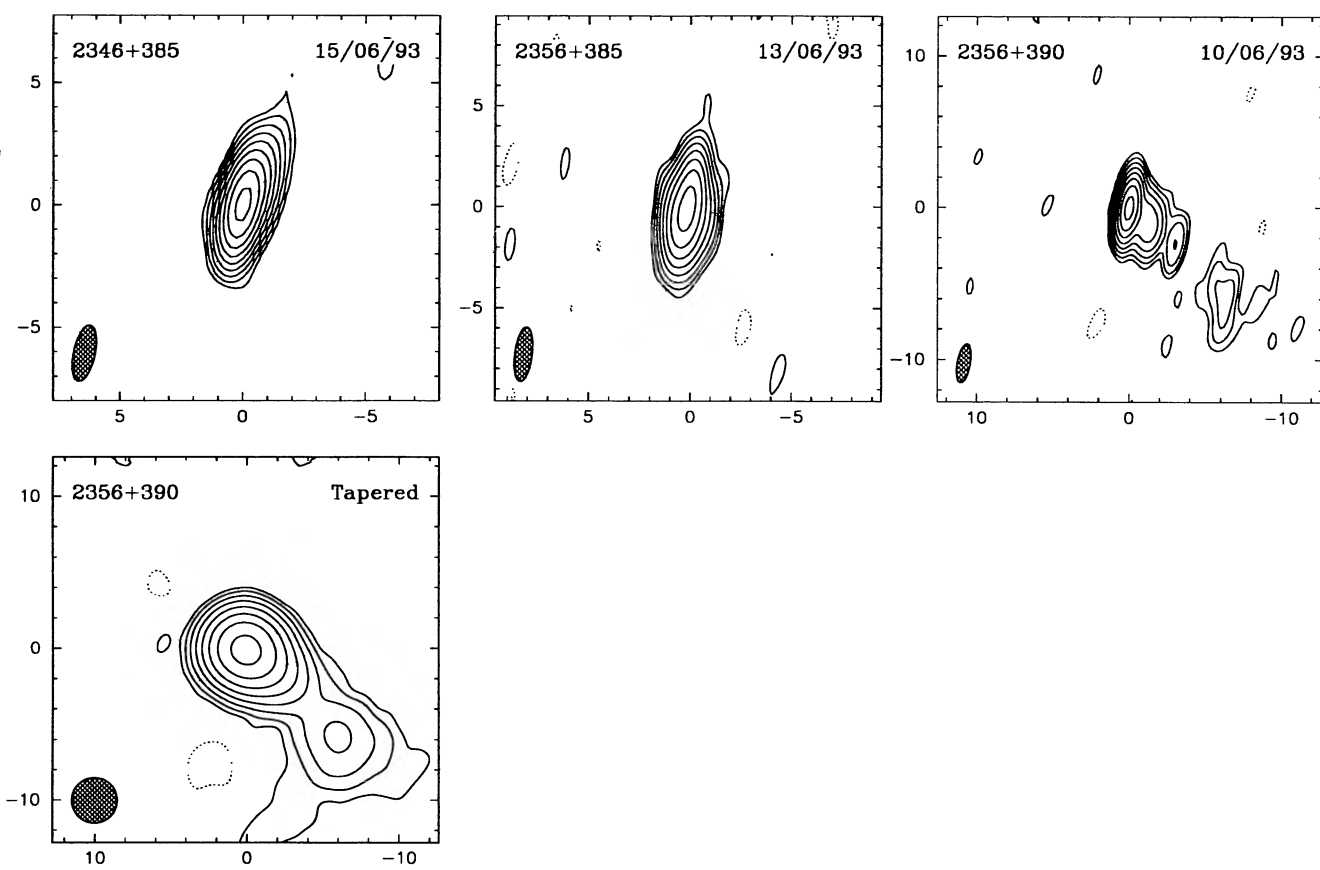
FIG. 2—*Continued*

TABLE 2
MAP PARAMETERS

Name	Dur.	Beam			θ (°)	S_{nat} (mJy/beam)	rms	1st Cntr	S_{tap} (mJy/beam)	rms	1st Cntr
		<i>a</i> (mas)	<i>b</i> (mas)	θ (mas)							
(1)	(2)	(3)	(4)	(5)	(6)	(7)	(8)	(9)	(10)	(11)	
0003+380...	57	2.17	0.92	-6	471	0.71	0.45				
0035+413...	62	2.24	0.92	3	530	0.61	0.35	869	0.63	0.20	
0109+351...	57	2.80	0.85	-4	332	0.56	0.50				
0110+495...	57	1.61	0.98	0	633	0.70	0.35				
0129+431...	57	1.92	0.94	-8	275	0.40	0.45				
0145+386...	57	2.21	0.91	-6	288	0.59	0.60				
0151+474...	81	1.72	0.94	-4	723	0.55	0.25				
0201+365...	76	2.66	0.82	-5	134	0.46	1.05				
0227+403...	57	2.22	0.91	-6	459	0.66	0.45				
0249+383...	57	2.27	0.89	-6	200	0.62	0.95				
0251+393...	56	2.19	0.92	-4	410	0.44	0.30				
0256+424...	59	1.93	0.88	-9	93	0.74	2.40	118	1.21	3.10	
0307+380...	95	2.41	0.90	0	490	0.41	0.25				
0309+411...	76	2.14	0.90	0	319	0.43	0.40				
0340+362...	76	2.56	0.88	-3	446	0.41	0.30	527	0.52	0.30	
0600+442...	57	1.88	1.04	-21	141	0.79	1.70	240	1.11	1.40	
0627+532...	76	1.79	0.98	20	152	0.63	1.25				
0641+393...	76	2.41	0.90	0	495	0.45	0.25				
0650+453...	57	1.68	1.03	2	415	0.57	0.40				
0651+410...	57	1.97	0.95	-9	257	0.62	0.70				
0700+470...	96	1.70	1.09	3	159	0.49	0.90	268	0.63	0.70	
0714+457...	57	1.72	0.99	-8	421	0.43	0.30				
0727+409...	57	2.02	0.98	-12	238	0.64	0.80	364	0.76	0.65	
0731+479...	57	1.61	1.00	-8	247	0.47	0.55				
0738+491...	57	1.46	1.07	-2	659	0.37	0.15				
0739+398...	76	2.37	0.91	-5	214	0.48	0.65	262	0.58	0.65	
0743+744...	57	1.21	1.01	22	327	0.59	0.55	416	0.83	0.60	
0803+452...	57	1.89	0.95	-5	230	0.46	0.60				
0824+355...	56	2.39	0.94	-7	400	0.42	0.30	512	0.58	0.35	
0830+425...	56	1.84	1.00	0	264	0.55	0.65	300	0.61	0.60	
0833+416...	57	2.38	0.92	-8	195	0.61	0.95				
0902+490...	58	1.73	0.98	-13	472	0.62	0.40				
0913+391...	57	2.26	0.94	-6	235	0.67	0.85				
0925+504...	97	1.60	1.07	-26	949	0.52	0.15	1020	1.02	0.30	
0927+352...	57	2.35	0.95	-6	223	0.70	0.95				
0930+493...	57	1.65	1.01	-23	293	0.69	0.70				
0933+503...	57	1.84	0.96	-7	136	0.62	1.35				
0941+522...	57	1.56	1.03	-1	293	0.43	0.45	341	0.54	0.50	
0942+468...	55	1.48	1.13	-6	220	0.78	1.05				
0949+354...	57	2.67	0.90	-4	273	0.55	0.60				
1010+350...	58	2.45	0.88	-9	227	0.56	0.75				
1030+398...	57	2.33	0.90	-8	432	0.50	0.35				
1038+528...	57	1.56	1.01	-6	639	0.55	0.25				
1041+536...	58	1.48	1.03	5	264	0.43	0.50				
1105+437...	57	1.92	0.96	-2	254	0.43	0.50	280	0.50	0.55	
1124+455...	57	2.15	0.91	-12	210	0.70	1.00				
1144+352...	57	2.50	0.90	-7	250	0.49	0.60	329	1.00	0.90	
1146+531...	57	1.49	1.00	-17	353	0.45	0.40	370	0.58	0.45	
1151+408...	57	2.25	0.90	-6	200	0.50	0.75	423	0.57	0.40	
1155+486...	57	1.55	1.08	-20	294	0.55	0.55	324	0.65	0.60	
1205+544...	57	1.47	1.13	-13	197	0.80	1.20				
1206+415...	57	2.07	0.91	-5	286	0.58	0.60				
1221+809...	57	1.13	1.03	57	239	0.44	0.55	297	0.65	0.65	
1223+395...	56	2.21	0.93	0	195	0.65	1.00	211	0.84	1.20	
1226+373...	57	2.35	0.92	-6	693	0.49	0.20	723	0.50	0.20	

TABLE 2—Continued

Name	Dur.	Beam			S_{nat}	rms	1st Cntr	S_{tap}	rms	1st Cntr	
		(1)	(2) (min)	(3) (mas)	(4) (mas)	(5) ($^{\circ}$)	(6) (mJy/beam)	(7)	(8) (%Peak)	(9) (mJy/beam)	(10)
1239+376...	57	1.97	1.07	-5	208	0.69	1.00				
1240+381...	57	2.29	0.95	-9	355	0.55	0.45	489	0.64	0.40	
1250+532...	57	1.44	1.02	-10	181	0.50	0.85				
1258+507...	57	1.56	1.04	-1	218	0.70	0.95				
1308+471...	57	1.81	0.97	-14	239	0.46	0.60				
1312+533...	57	1.71	0.99	-31	292	0.52	0.55				
1321+410...	57	2.00	0.97	-21	181	0.63	1.05				
1325+436...	76	1.99	0.93	-19	371	0.48	0.40				
1413+373...	76	2.45	0.92	-12	224	0.54	0.70				
1415+463...	57	1.85	0.93	-16	234	0.67	0.85				
1417+385...	57	2.25	0.88	-11	560	0.56	0.30				
1421+482...	57	1.83	0.91	-16	287	0.56	0.60				
1424+366...	76	2.36	0.90	-13	627	0.45	0.20	719	0.60	0.25	
1427+543...	57	1.52	0.98	-28	340	0.61	0.55	410	0.76	0.55	
1448+762...	57	1.20	1.00	-79	300	0.50	0.50				
1456+375...	57	2.32	0.88	-13	698	0.55	0.25				
1459+480...	57	1.76	0.98	-39	392	0.71	0.55	433	1.15	0.80	
1505+428...	57	1.92	0.92	-16	309	0.53	0.50				
1534+501...	76	1.76	0.93	-22	226	0.53	0.70				
1543+480...	57	1.85	0.90	-14	283	0.50	0.55				
1543+517...	76	1.53	0.96	-17	404	0.46	0.35	479	0.56	0.35	
1545+497...	57	1.55	0.98	-25	24	0.43	5.40				
1550+582...	57	1.43	0.95	-31	211	0.49	0.70				
1602+576...	57	1.45	0.96	-18	212	0.63	0.90				
1619+491...	57	1.70	0.95	-22	211	0.45	0.65	282	0.58	0.60	
1629+495...	57	1.77	0.92	-26	366	0.67	0.55				
1636+473...	57	1.92	0.92	-28	547	0.78	0.45				
1638+540...	76	1.36	1.03	-20	171	0.48	0.85				
1645+410...	57	2.33	0.89	-14	497	0.56	0.35				
1722+401...	57	2.00	0.94	-14	283	0.57	0.60	319	0.83	0.80	
1726+455...	57	1.83	0.92	-14	1080	0.82	0.25				
1734+363...	57	2.59	0.88	-15	392	0.55	0.40				
1742+402...	57	3.69	1.20	-9	139	0.79	1.70	182	0.90	1.50	
1747+433...	95	2.05	0.91	-7	262	0.39	0.45	269	0.53	0.60	
1812+412...	57	2.11	0.91	-19	256	0.52	0.60	272	0.84	0.95	
1828+399...	76	2.40	0.84	-13	213	0.45	0.65				
1839+389...	76	2.57	0.86	-12	204	0.42	0.60				
1850+402...	58	2.02	0.92	-15	244	0.85	1.05				
1910+375...	57	2.25	0.90	-9	307	0.49	0.50	349	0.61	0.50	
1915+657...	76	1.24	1.03	-53	241	0.46	0.55				
1924+507...	76	1.35	1.05	-13	289	0.58	0.60	341	0.84	0.75	
2310+385...	57	2.34	0.95	-8	182	0.65	1.05				
2319+444...	97	2.09	0.88	-13	495	0.50	0.30				
2330+387...	58	2.30	0.89	-12	179	0.46	0.75	243	0.73	0.90	
2346+385...	57	2.34	0.88	-12	592	0.58	0.30				
2356+385...	76	2.72	0.85	-7	243	0.47	0.60				
2356+390...	76	2.58	0.85	-10	212	0.44	0.60	244	0.48	0.60	

NOTES.—Col. (2): Total integration time on source in minutes. Cols. (3)–(5): The beam characteristics of the naturally weighted maps. The restoring beam is an elliptical Gaussian with FWHM major axis a mas and minor axis b mas, with major axis in position angle θ° . Col. (6): The peak intensity of the naturally weighted maps (mJy beam $^{-1}$). Col. (7): The rms noise in the naturally weighted maps (mJy beam $^{-1}$), measured in the four corners of the displayed image. Col. (8): The lowest contour level of the map in percentage of the peak flux density. Cols. (9)–(11): The peak intensity, rms noise, and lowest contour level of the tapered map, if an image has been provided. All tapered maps have been restored with a 3 mas beam.

Table 2 is published in computer-readable form in the AAS CD-ROM Series, Vol. 4.

TABLE 3
GAUSSIAN MODELS

Source	<i>S</i> (Jy)	<i>r</i> (mas)	θ ($^{\circ}$)	<i>a</i> (mas)	<i>b/a</i>	Φ ($^{\circ}$)	Amplitude A.F.	Cl. Phase A.F.	Total A.F.
0003+380 ...	0.526	0.00	0.0	0.69	0.46	114.4	1.000	1.063	1.028
	0.183	0.89	122.4	0.61	0.14	146.2			
	0.013	4.62	111.9	1.67	0.53	7.4			
0035+413 ...	0.456	0.00	0.0	0.57	0.00	99.1	1.024	1.154	1.084
	0.474	0.83	95.8	0.60	0.50	-36.4			
	0.017	3.80	101.8	1.46	0.00	23.3			
	0.067	9.62	112.9	10.14	0.29	127.0			
0109+351 ...	0.300	0.00	0.0	0.45	0.00	-155.9	1.025	1.042	1.033
	0.065	0.58	-163.9	0.96	0.26	-150.3			
	0.014	5.54	-156.3	7.00	0.09	-155.8			
0110+495 ...	0.666	0.00	0.0	0.67	0.23	-27.8	1.012	1.093	1.049
	0.131	1.05	-39.8	2.78	0.29	-37.4			
	0.094	8.33	-30.9	4.11	0.46	0.1			
0129+431 ...	0.289	0.00	0.0	0.49	0.39	159.5	1.001	1.022	1.010
	0.013	1.95	-7.5	3.11	0.16	28.9			
0145+386 ...	0.401	0.00	0.0	0.95	0.61	122.1	0.917	1.153	1.030
	0.057	1.18	-45.5	0.85	0.32	23.6			
0151+474 ...	0.762	0.00	0.0	0.43	0.51	16.3	0.876	1.012	0.939
	0.036	1.67	-178.6	0.76	0.54	-3.8			
0201+365 ...	0.144	0.00	0.0	0.34	0.59	45.7	1.016	1.165	1.085
	0.108	2.45	-3.5	1.03	0.45	-11.7			
	0.035	7.24	-3.8	3.54	0.60	4.9			
0227+403 ...	0.502	0.00	0.0	0.75	0.39	162.1	0.950	1.053	0.997
	0.048	2.38	138.6	2.63	0.10	120.8			
0249+383 ...	0.199	0.00	0.0	0.61	0.86	165.1	1.050	1.042	1.047
	0.107	1.47	-12.8	2.01	0.37	-31.1			
	0.056	5.15	-19.7	3.44	0.33	-28.7			
0251+393 ...	0.438	0.00	0.0	0.43	0.35	90.9	0.977	1.016	0.994
	0.048	0.75	80.6	1.20	0.71	10.2			
	0.008	9.13	65.1	1.40	0.00	48.8			
0256+424 ...	0.113	0.00	0.0	0.74	0.00	35.0	1.040	1.244	1.135
	0.151	10.34	65.4	1.39	0.60	-51.8			
	0.106	4.57	55.7	1.74	0.46	-86.9			
0307+380 ...	0.515	0.00	0.0	0.32	0.44	80.2	0.915	1.002	0.955
	0.006	3.57	68.7	0.80	0.80	47.7			
0309+411 ...	0.318	0.00	0.0	0.44	0.82	135.9	0.895	1.029	0.957
	0.112	0.91	-51.5	1.19	0.00	-62.8			
	0.031	3.74	-55.2	3.26	0.00	-61.7			
0340+362 ...	0.470	0.00	0.0	0.53	0.55	54.8	0.896	1.039	0.963
	0.081	0.85	31.8	0.87	0.90	80.8			
	0.008	9.52	21.0	4.28	0.18	145.1			
0600+442 ...	0.222	0.00	0.0	1.08	0.70	-69.4	1.027	1.211	1.112
	0.159	2.52	-49.6	2.44	0.75	-26.6			
	0.080	5.04	-35.3	5.38	0.67	12.3			
0627+532 ...	0.215	0.00	0.0	1.21	0.23	65.6	1.043	1.146	1.090
	0.093	2.81	-132.1	0.77	0.01	-160.1			
	0.151	2.68	66.7	2.27	0.33	48.9			
	0.026	8.94	52.1	3.01	0.36	46.6			

TABLE 3—Continued

Source	<i>S</i> (Jy)	<i>r</i> (mas)	θ ($^{\circ}$)	<i>a</i> (mas)	<i>b/a</i>	Φ ($^{\circ}$)	Amplitude A.F.	Cl. Phase A.F.	Total A.F.
0641+393 ...	0.498	0.00	0.0	0.42	0.40	19.1	0.902	1.026	0.960
	0.063	1.77	-7.4	4.02	0.21	-1.6			
	0.016	4.70	1.4	3.05	0.13	32.1			
0650+453 ...	0.431	0.00	0.0	0.29	0.73	135.5	0.901	1.037	0.965
	0.037	1.04	100.1	2.17	0.39	53.2			
0651+410 ...	0.308	0.00	0.0	1.12	0.27	166.0	0.866	1.052	0.954
	0.033	1.56	156.4	0.79	0.00	72.4			
0700+470 ...	0.280	0.00	0.0	1.59	0.44	-24.2	1.084	1.310	1.188
	0.123	2.44	122.6	2.71	0.34	102.2			
	0.098	7.05	93.1	6.16	0.34	64.2			
	0.012	21.21	77.9	7.32	0.00	138.8			
0714+457 ...	0.424	0.00	0.0	0.41	0.08	148.7	0.909	1.047	0.974
	0.095	2.02	124.8	4.66	0.17	127.2			
	0.005	17.46	117.5	1.48	0.24	23.0			
0727+409 ...	0.213	0.00	0.0	0.49	0.57	-44.8	1.024	1.203	1.106
	0.197	1.12	124.1	0.74	0.44	139.3			
	0.007	2.89	-51.9	0.02	0.91	35.4			
0731+479 ...	0.231	0.00	0.0	0.37	0.72	61.1	1.009	1.063	1.034
	0.182	1.02	-103.6	0.84	0.34	-83.3			
	0.093	2.40	-87.9	1.87	0.08	-98.3			
	0.006	8.86	-85.7	1.01	0.38	-16.9			
0738+491 ...	0.691	0.00	0.0	0.28	0.94	174.1	0.879	1.009	0.939
0739+398 ...	0.209	0.00	0.0	0.76	0.38	161.6	1.000	1.080	1.037
	0.103	1.53	158.2	0.70	0.52	142.5			
	0.030	5.88	140.6	8.31	0.25	120.9			
0743+744 ...	0.368	0.00	0.0	0.71	0.20	24.8	0.891	1.064	0.972
	0.091	1.18	28.6	0.75	0.00	-17.9			
	0.015	5.32	28.5	1.88	0.33	127.9			
0803+452 ...	0.374	0.00	0.0	1.26	0.28	-125.8	0.997	1.207	1.096
0824+355 ...	0.009	2.03	-123.6	0.00	0.55	125.4			
	0.131	11.07	52.8	22.05	0.19	52.7			
0830+425 ...	0.299	0.00	0.0	0.57	0.41	-74.9	0.994	1.040	1.015
	0.034	3.72	-84.1	6.02	0.00	-86.8			
0833+416 ...	0.238	0.00	0.0	1.41	0.24	5.0	0.987	1.162	1.069
	0.083	2.12	-171.9	0.44	0.05	-28.0			
0902+490 ...	0.480	0.00	0.0	0.39	0.76	-32.6	0.940	1.065	0.998
	0.141	1.18	-39.8	0.76	0.95	-37.8			
0913+391 ...	0.276	0.00	0.0	0.74	0.77	28.0	0.945	1.088	1.011
	0.125	2.32	-114.9	1.00	0.87	9.11			
	0.133	3.37	-97.9	1.13	0.74	29.1			
0925+504 ...	1.032	0.00	0.0	0.51	0.36	107.2	0.918	1.029	0.969
	0.035	5.24	126.4	7.65	0.24	128.5			
0927+352 ...	0.242	0.00	0.0	0.49	0.69	138.9	1.038	1.079	1.056
	0.078	4.36	103.0	3.95	0.43	102.1			
0930+493 ...	0.483	0.00	0.0	1.17	0.55	-133.6	0.863	1.122	0.985
	0.076	2.57	-136.3	1.12	0.30	-143.1			

TABLE 3—Continued

Source	<i>S</i> (Jy)	<i>r</i> (mas)	θ (°)	<i>a</i> (mas)	<i>b/a</i>	Φ (°)	Amplitude A.F.	Cl. Phase A.F.	Total A.F.
0933+503 ...	0.127	0.00	0.0	0.06	0.00	127.2	0.972	1.079	1.021
	0.065	0.92	64.0	0.92	0.43	58.4			
0941+522 ...	0.350	0.00	0.0	0.80	0.44	165.8	0.975	1.117	1.041
	0.122	3.50	150.8	1.21	0.65	166.4			
	0.074	5.82	163.9	6.45	0.13	158.0			
	0.009	30.82	175.4	1.57	0.00	118.0			
0942+468 ...	0.229	0.00	0.0	0.59	0.50	62.1	0.981	1.068	1.021
	0.075	1.01	47.4	0.68	0.56	14.8			
	0.049	2.62	31.1	1.94	0.71	72.0			
0949+354 ...	0.296	0.00	0.0	0.99	0.27	168.9	0.988	1.164	1.071
	0.078	3.11	167.0	5.11	0.13	169.9			
1010+350 ...	0.233	0.00	0.0	0.26	0.57	50.6	0.876	1.003	0.935
	0.088	1.83	98.0	1.22	0.70	32.0			
	0.033	5.40	99.1	4.47	0.22	78.6			
1030+398 ...	0.577	0.00	0.0	1.10	0.13	35.0	0.907	1.090	0.994
	0.108	2.04	47.6	0.95	0.33	87.4			
	0.007	7.58	40.9	0.61	0.00	65.1			
1038+528 ...	0.667	0.00	0.0	0.48	0.12	16.2	0.906	1.063	0.979
	0.055	1.25	27.1	0.16	0.17	132.8			
	0.027	2.71	18.3	3.88	0.24	27.4			
1041+536 ...	0.346	0.00	0.0	0.97	0.33	145.3	0.996	1.045	1.019
	0.053	2.58	160.1	3.28	0.34	178.7			
1105+437 ...	0.246	0.00	0.0	0.26	0.00	-133.5	1.000	1.049	1.022
	0.055	0.98	-136.5	1.45	0.47	-138.7			
	0.012	8.66	-125.6	3.27	0.29	-26.3			
1124+455 ...	0.213	0.00	0.0	0.81	0.00	-25.5	1.009	1.195	1.096
	0.145	2.48	-5.0	2.37	0.12	0.5			
1144+352 ...	0.297	0.00	0.0	0.60	0.86	31.9	0.962	1.159	1.055
	0.170	2.66	-58.2	3.99	0.86	-55.3			
	0.071	21.67	-58.5	0.55	0.78	-49.2			
1146+531 ...	0.378	0.00	0.0	0.37	0.70	122.4	0.884	1.046	0.960
1151+408 ...	0.365	0.00	0.0	1.08	0.83	64.3	0.919	1.184	1.047
	0.181	1.66	73.1	0.92	0.00	88.3			
1155+486 ...	0.310	0.00	0.0	0.46	0.40	-78.7	0.889	1.068	0.972
	0.041	1.53	-100.5	2.40	0.31	-132.0			
1205+544 ...	0.284	0.00	0.0	1.00	0.63	105.6	0.949	1.153	1.045
	0.141	2.48	121.5	0.91	0.32	58.2			
1206+415 ...	0.327	0.00	0.0	0.53	0.68	40.5	0.903	1.019	0.957
	0.007	16.36	-162.8	0.63	0.00	-54.7			
1221+809 ...	0.239	0.00	0.0	0.33	0.33	-22.2	0.887	1.036	0.956
	0.074	1.02	-3.5	0.65	0.63	-19.1			
	0.093	6.12	-6.6	6.06	0.18	-11.7			
1223+395 ...	0.206	0.00	0.0	0.56	0.41	18.6	0.906	1.188	1.041
	0.016	3.22	35.6	3.01	0.35	14.6			
	0.217	7.55	34.7	1.34	0.43	8.1			
	0.067	12.64	27.0	6.51	0.26	46.0			

TABLE 3—Continued

Source	<i>S</i> (Jy)	<i>r</i> (mas)	θ (°)	<i>a</i> (mas)	<i>b/a</i>	Φ (°)	Amplitude A.F.	Cl. Phase A.F.	Total A.F.
1226+373 ...	0.729 0.012	0.00 3.17	0.0 −70.7	0.34 2.09	0.67 0.00	−51.4 −127.9	0.886	1.014	0.946
1239+376 ...	0.231 0.189	0.00 1.54	0.0 −159.8	1.51 0.80	0.34 0.78	2.3 107.7	0.863	1.100	0.974
1240+381 ...	0.526	0.00	0.0	1.08	0.45	−66.3	0.892	1.106	0.994
1250+532 ...	0.207 0.063	0.00 4.28	0.0 −100.4	0.59 5.53	0.19 0.24	−120.1 −96.4	0.922	1.073	0.992
1258+507 ...	0.194 0.152	0.00 1.30	0.0 162.9	0.20 0.63	0.83 0.50	82.9 159.8	0.887	1.110	0.992
1308+471 ...	0.256	0.00	0.0	0.38	0.72	24.6	0.851	1.038	0.939
1312+533 ...	0.300 0.170	0.00 1.53	0.0 −118.4	0.27 1.01	0.80 0.47	1.5 −110.8	0.863	1.047	0.950
1321+410 ...	0.226 0.187	0.00 5.42	0.0 −82.5	0.62 0.74	0.93 0.85	−90.9 20.1	0.865	1.194	1.022
1325+436 ...	0.403 0.181	0.00 0.78	0.0 −139.0	0.75 0.85	0.43 0.92	40.4 −173.3	0.896	1.118	1.001
1413+373 ...	0.263 0.096 0.023 0.010	0.00 1.56 1.65 4.25	0.0 −44.7 116.9 116.5	0.77 0.23 0.72 0.54	0.15 0.00 0.26 0.01	109.9 −1.0 21.2 29.7	0.889	1.088	0.983
1415+463 ...	0.234 0.232 0.043 0.155	0.00 1.14 2.53 10.47	0.0 76.2 −95.3 −97.5	0.41 1.02 1.12 0.84	0.82 0.00 0.59 0.73	46.9 87.0 −3.3 −54.4	0.901	1.125	1.007
1417+385 ...	0.619	0.00	0.0	0.41	0.92	−10.7	0.972	1.036	1.001
1421+482 ...	0.324 0.074	0.00 2.24	0.0 −73.0	0.52 2.62	0.75 0.64	−100.0 −72.9	0.864	1.087	0.971
1424+366 ...	0.669 0.090	0.00 1.13	0.0 −129.6	0.40 0.52	0.71 0.00	27.2 −37.7	0.874	1.036	0.950
1427+543 ...	0.351 0.100 0.038	0.00 1.28 6.20	0.0 136.7 141.5	0.58 0.76 7.43	0.37 0.54 0.16	138.4 119.9 154.4	0.941	1.043	0.987
1448+762 ...	0.318 0.088	0.00 0.77	0.0 81.5	0.66 1.08	0.19 0.43	78.5 82.8	0.845	1.063	0.947
1456+375 ...	0.737 0.045	0.00 1.36	0.0 112.8	0.30 1.42	0.98 0.56	168.9 9.4	0.900	1.077	0.983
1459+480 ...	0.400 0.067 0.059	0.00 1.43 6.66	0.0 86.0 72.9	0.36 1.74 5.97	0.25 0.19 0.10	40.4 82.0 50.4	0.870	1.066	0.962
1505+428 ...	0.373 0.042 0.037	0.00 1.17 5.00	0.0 −97.8 −103.8	0.62 0.00 4.35	0.54 0.70 0.00	−101.5 −95.2 −109.0	0.892	1.058	0.970
1534+501 ...	0.315	0.00	0.0	1.43	0.13	−35.4	0.947	1.277	1.108

TABLE 3—Continued

Source	<i>S</i> (Jy)	<i>r</i> (mas)	θ (°)	<i>a</i> (mas)	<i>b/a</i>	Φ (°)	Amplitude A.F.	Cl. Phase A.F.	Total A.F.
1543+480 ...	0.299	0.00	0.0	0.46	0.80	97.8	0.914	1.051	0.978
	0.116	1.49	141.3	1.23	0.54	141.9			
	0.079	34.93	115.6	0.68	0.93	63.6			
1543+517 ...	0.358	0.00	0.0	0.42	0.52	177.9	0.893	1.044	0.964
	0.131	0.74	173.2	0.59	0.33	57.0			
	0.055	2.26	-169.4	1.15	0.54	23.4			
	0.022	5.34	179.4	1.19	0.62	120.3			
	0.057	23.39	172.1	8.21	0.24	149.9			
1545+497 ...	0.041	0.00	0.0	0.44	0.30	37.1	0.876	1.141	1.002
1550+582 ...	0.195	0.00	0.0	0.49	0.23	160.5	0.847	1.026	0.931
	0.093	1.03	163.2	1.33	0.00	143.6			
1602+576 ...	0.278	0.00	0.0	0.92	0.34	140.1	0.902	1.086	0.988
	0.076	3.87	130.9	0.53	0.67	12.2			
1619+491 ...	0.236	0.00	0.0	0.66	0.40	5.7	0.892	1.075	0.978
	0.087	1.30	9.0	0.47	0.01	96.6			
	0.052	6.51	2.5	1.66	0.59	38.4			
	0.033	10.26	8.2	3.75	0.63	-81.1			
1629+495 ...	0.415	0.00	0.0	0.53	0.31	-112.4	0.890	1.050	0.965
	0.033	1.12	-114.9	0.55	0.91	-8.1			
1636+473 ...	0.705	0.00	0.0	1.48	0.17	-20.7	1.048	1.086	1.065
	0.045	5.85	-31.3	6.99	0.15	-25.3			
1638+540 ...	0.229	0.00	0.0	0.79	0.72	-147.3	0.821	1.106	0.957
	0.056	1.22	-156.2	0.34	0.46	-31.9			
1645+410 ...	0.465	0.00	0.0	0.19	0.34	128.8	0.873	1.011	0.937
	0.085	0.89	136.1	0.81	0.60	111.5			
	0.020	2.22	132.2	0.60	0.00	98.8			
1722+401 ...	0.336	0.00	0.0	0.73	0.52	131.7	0.949	1.078	1.009
	0.055	4.41	-53.4	2.88	0.44	-44.6			
1726+455 ...	1.109	0.00	0.0	0.32	0.98	-80.0	0.932	1.042	0.983
	0.198	0.96	-76.5	0.92	0.62	-74.0			
1734+363 ...	0.534	0.00	0.0	0.80	0.59	71.7	0.873	1.041	0.952
1742+402 ...	0.217	0.00	0.0	1.20	0.83	15.3	0.845	1.259	1.031
	0.116	4.77	-94.6	2.57	0.54	-89.3			
	0.053	11.04	-104.5	4.68	0.63	-90.2			
1747+433 ...	0.252	0.00	0.0	0.10	0.00	104.0	0.883	1.036	0.955
	0.022	0.94	-171.2	1.10	0.00	-16.1			
	0.011	3.40	179.0	0.74	0.76	4.0			
	0.055	13.29	167.1	2.35	0.55	115.0			
1812+412 ...	0.275	0.00	0.0	0.41	0.83	138.0	0.881	1.038	0.954
	0.023	4.24	83.5	2.12	0.21	107.4			
	0.034	11.24	85.4	5.39	0.42	68.8			
1828+399 ...	0.222	0.00	0.0	0.44	0.79	-112.4	0.841	1.068	0.949
	0.072	0.98	-59.8	0.98	0.23	-62.5			
1839+389 ...	0.220	0.00	0.0	0.35	0.87	128.7	0.861	1.069	0.960
1850+402 ...	0.272	0.00	0.0	0.92	0.37	55.0	0.859	1.204	1.025
	0.376	1.41	61.8	1.64	0.19	69.2			

TABLE 3—Continued

Source	<i>S</i> (Jy)	<i>r</i> (mas)	θ (°)	<i>a</i> (mas)	<i>b/a</i>	Φ (°)	Amplitude A.F.	Cl. Phase A.F.	Total A.F.
1910+375 ...	0.388 0.021	0.00 7.52	0.0 177.5	1.33 3.32	0.25 0.26	159.8 −49.5	0.892	1.045	0.964
1915+657 ...	0.306 0.045 0.015	0.00 2.68 32.61	0.0 −54.4 −111.8	0.63 2.56 0.86	0.78 0.46 0.60	31.1 11.1 7.7	0.898	1.068	0.978
1924+507 ...	0.301 0.110 0.011	0.00 2.00 8.41	0.0 −0.4 3.0	0.50 1.26 3.11	0.23 0.26 0.38	1.0 −1.9 77.2	0.878	1.017	0.943
2310+385 ...	0.296 0.070 0.145	0.00 1.57 4.39	0.0 −131.1 59.2	1.21 1.90 1.36	0.36 0.00 0.46	−121.1 −167.9 50.1	0.876	1.190	1.026
2319+444 ...	0.509 0.038	0.00 2.13	0.0 −16.5	0.26 0.70	0.61 0.39	2.5 −7.8	0.873	1.007	0.935
2330+387 ...	0.250 0.033 0.182	0.00 1.68 45.20	0.0 −161.0 −151.9	1.00 0.00 4.44	0.58 0.80 0.49	24.8 0.0 −144.9	1.037	1.230	1.126
2346+385 ...	0.621 0.034	0.00 1.91	0.0 −28.7	0.44 0.66	0.23 0.00	−47.3 51.7	0.905	1.029	0.962
2356+385 ...	0.342 0.038	0.00 0.98	0.0 −136.4	1.67 0.826	0.30 0.00	−21.4 31.5	0.893	1.232	1.059
2356+390 ...	0.214 0.057 0.012 0.031	0.00 1.71 3.71 8.82	0.0 −129.2 −128.9 −134.9	0.26 1.07 0.64 4.14	0.93 0.31 0.00 0.83	51.1 −139.0 −95.2 −130.7	0.916	1.073	0.990

NOTES.—Parameters of each Gaussian component of the model brightness distribution: *S*, flux density; *r*, polar coordinates of the center of the component relative to an arbitrary origin, with polar angle measured from north through east; *a*, *b*, major and minor axes (FWHM); Φ , position angle of the major axis measured from north through east.

Table 3 is published in computer-readable form in the AAS CD-ROM Series, Vol. 4.

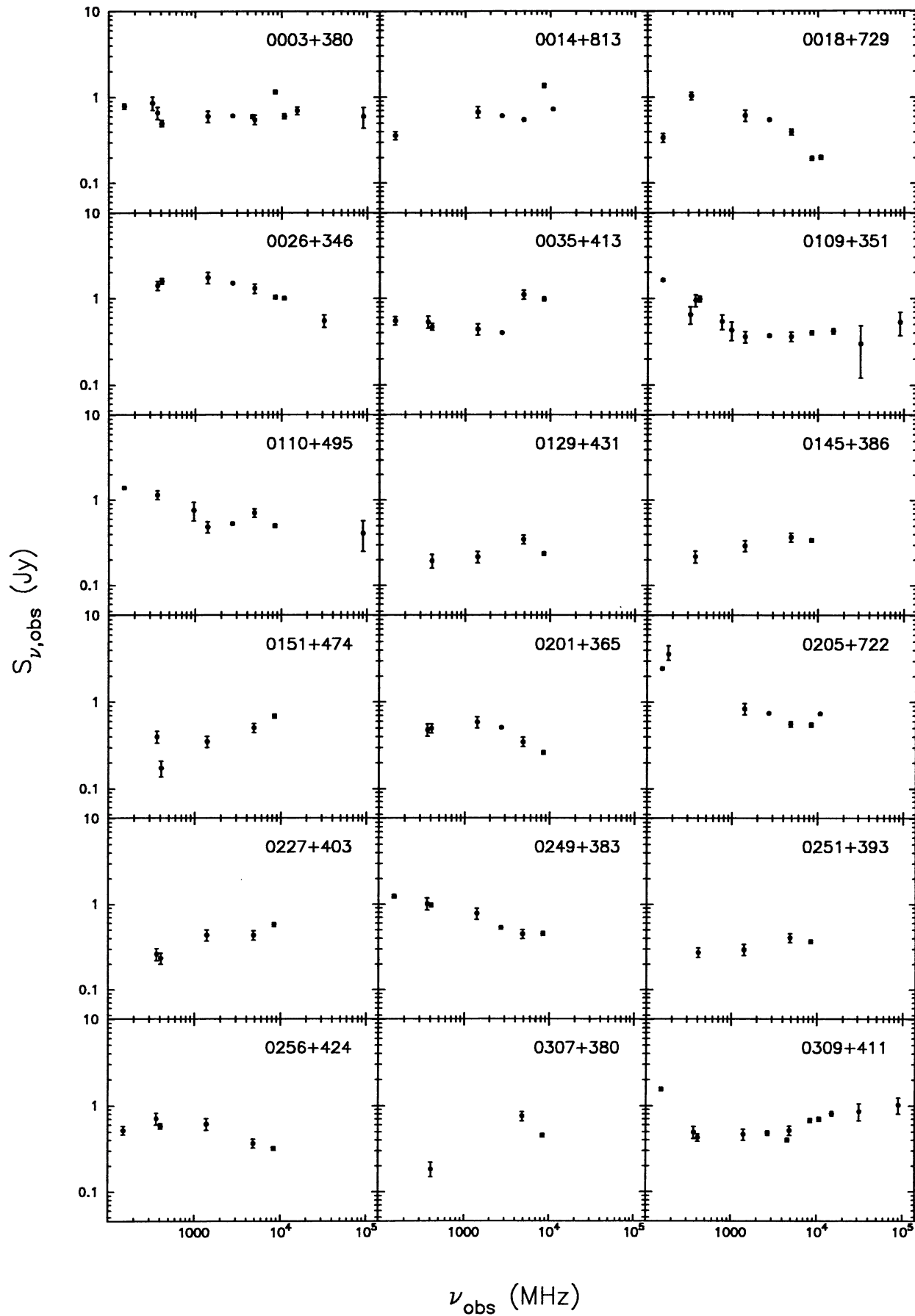


FIG. 3.—Integrated radio spectra for the entire CJ2 sample. All flux densities are on the scale of Laing & Peacock (1980). The error bars are $\pm 1 \sigma$ and are mainly taken from the flux density catalogs, although we have estimated some of these.

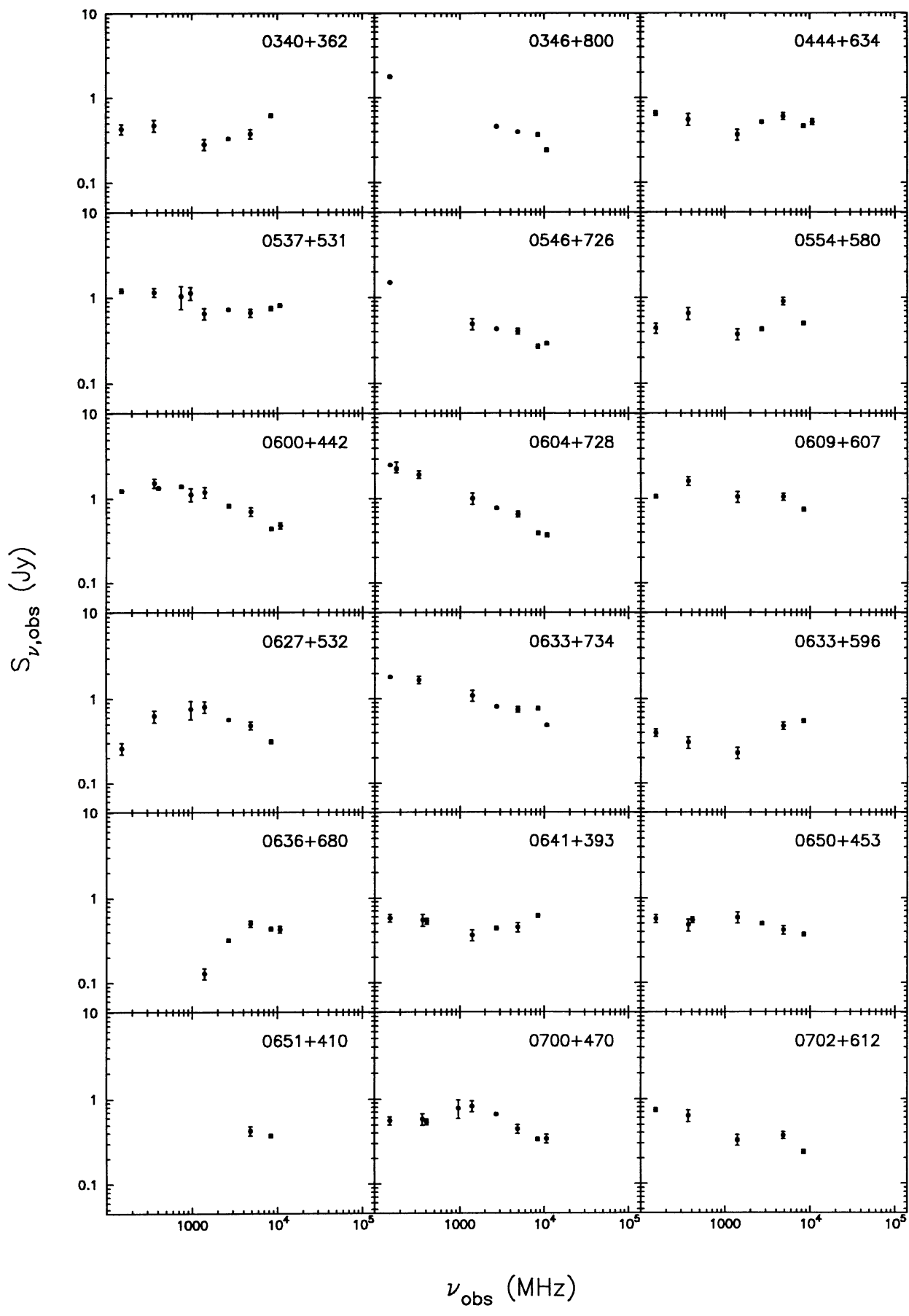


FIG. 3—Continued

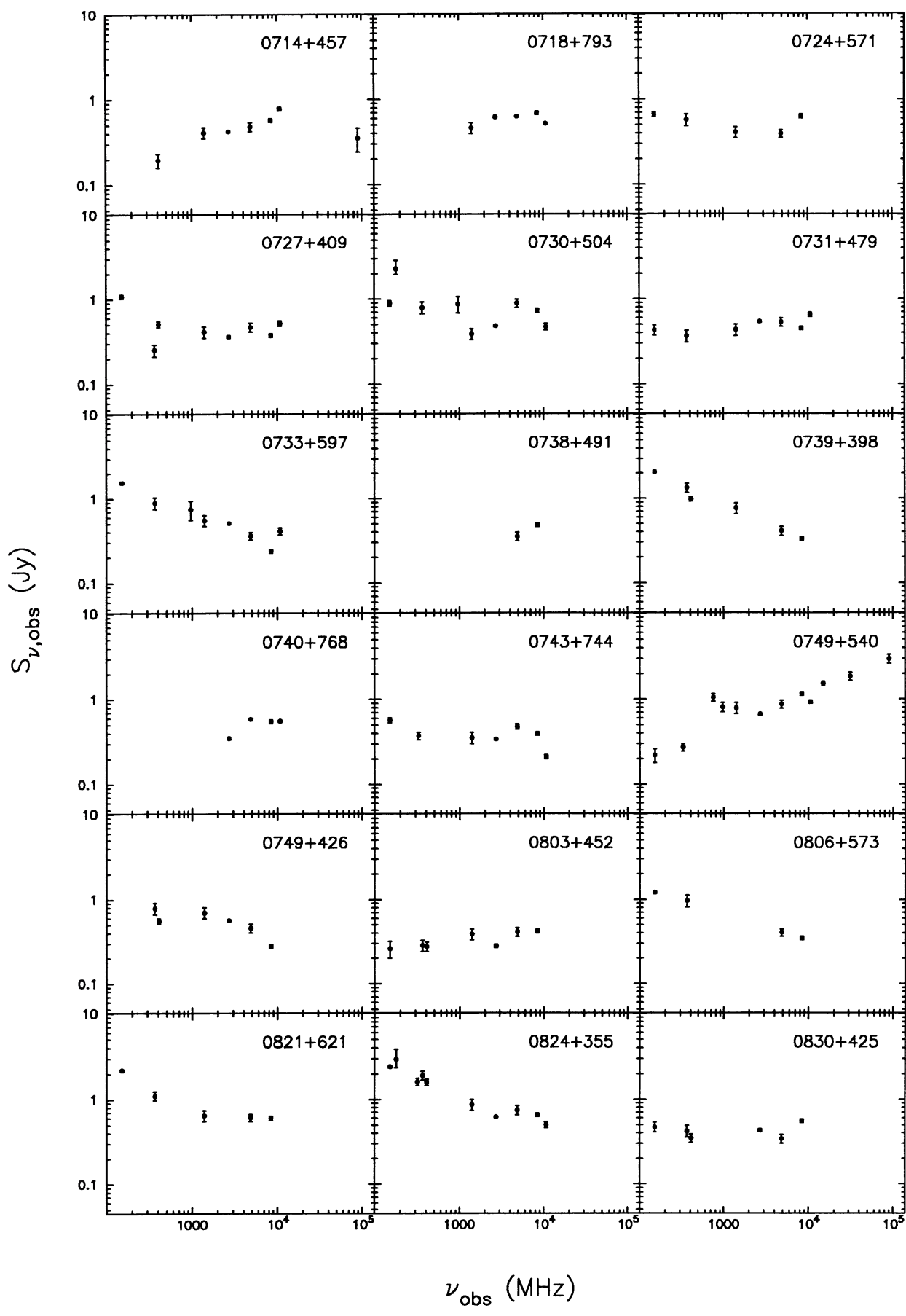


FIG. 3—Continued

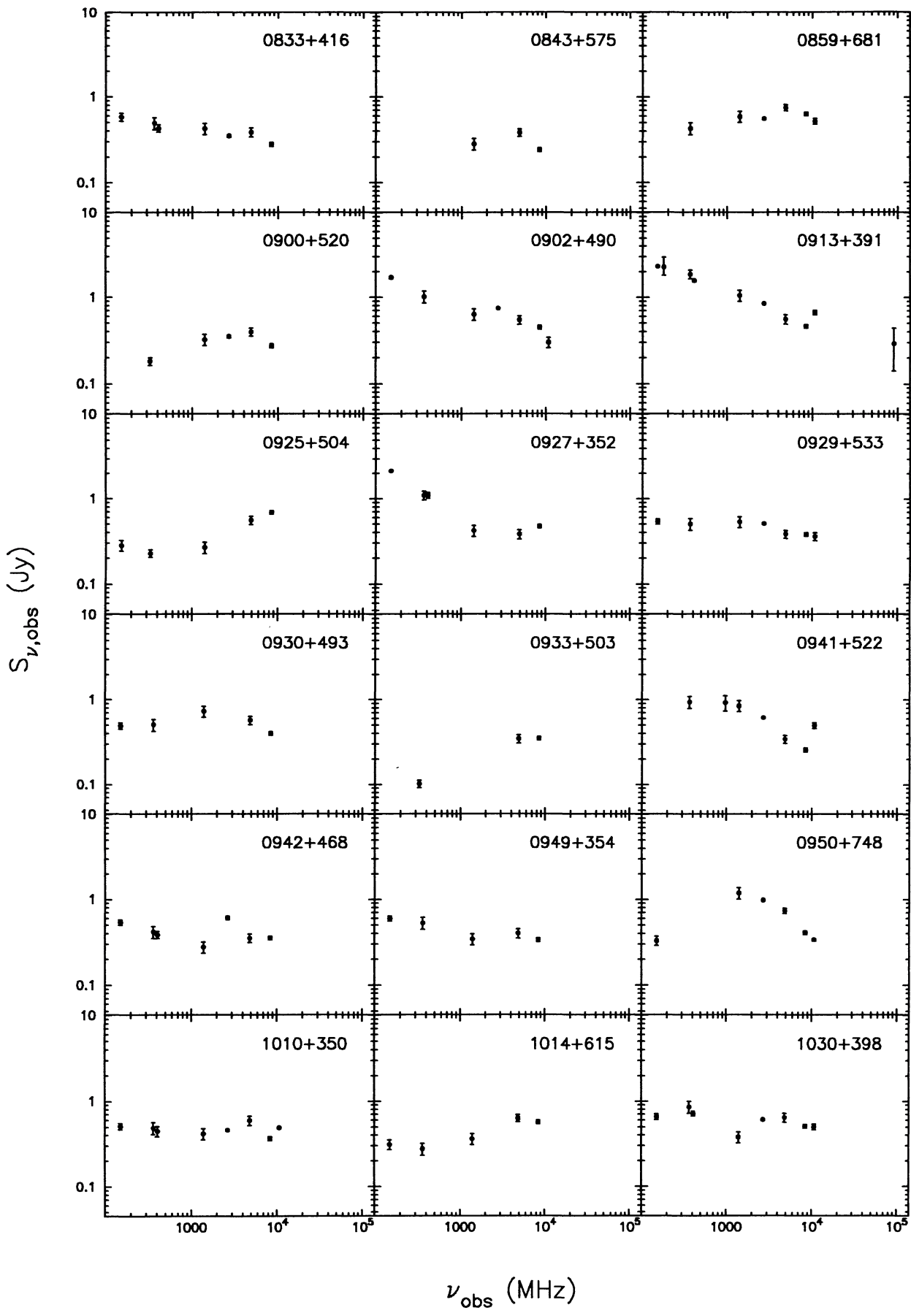


FIG. 3—Continued

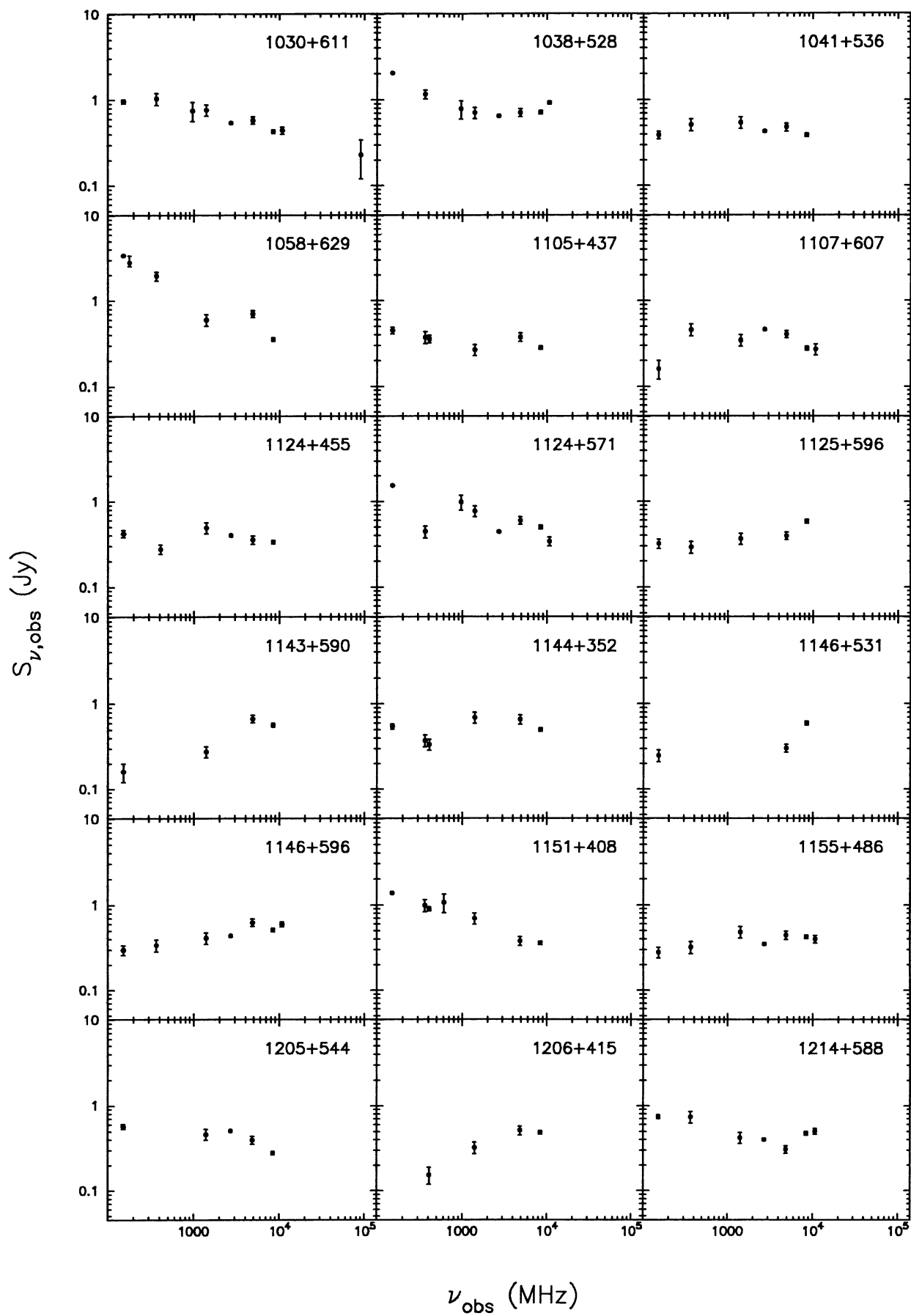


FIG. 3—Continued

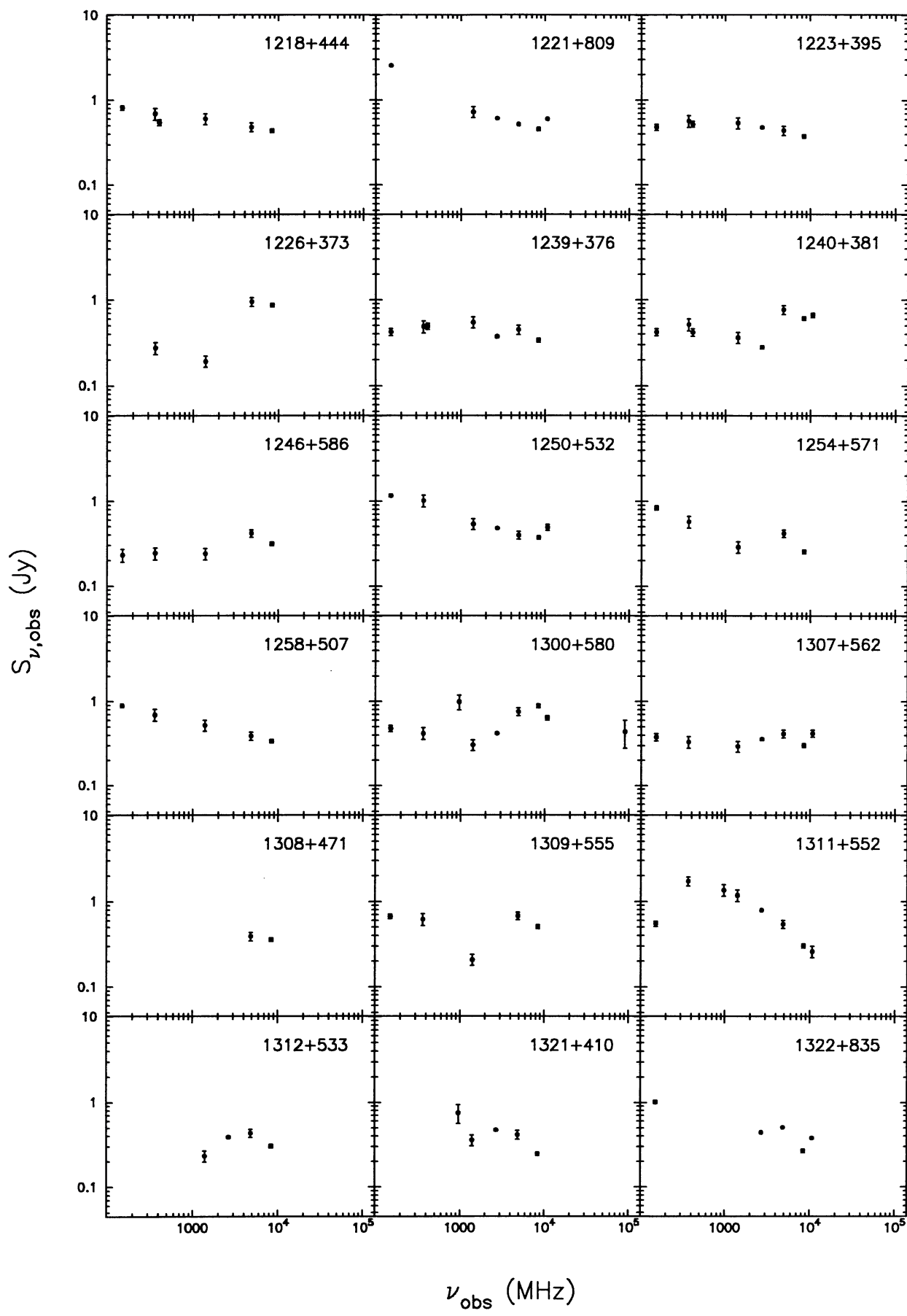


FIG. 3—Continued

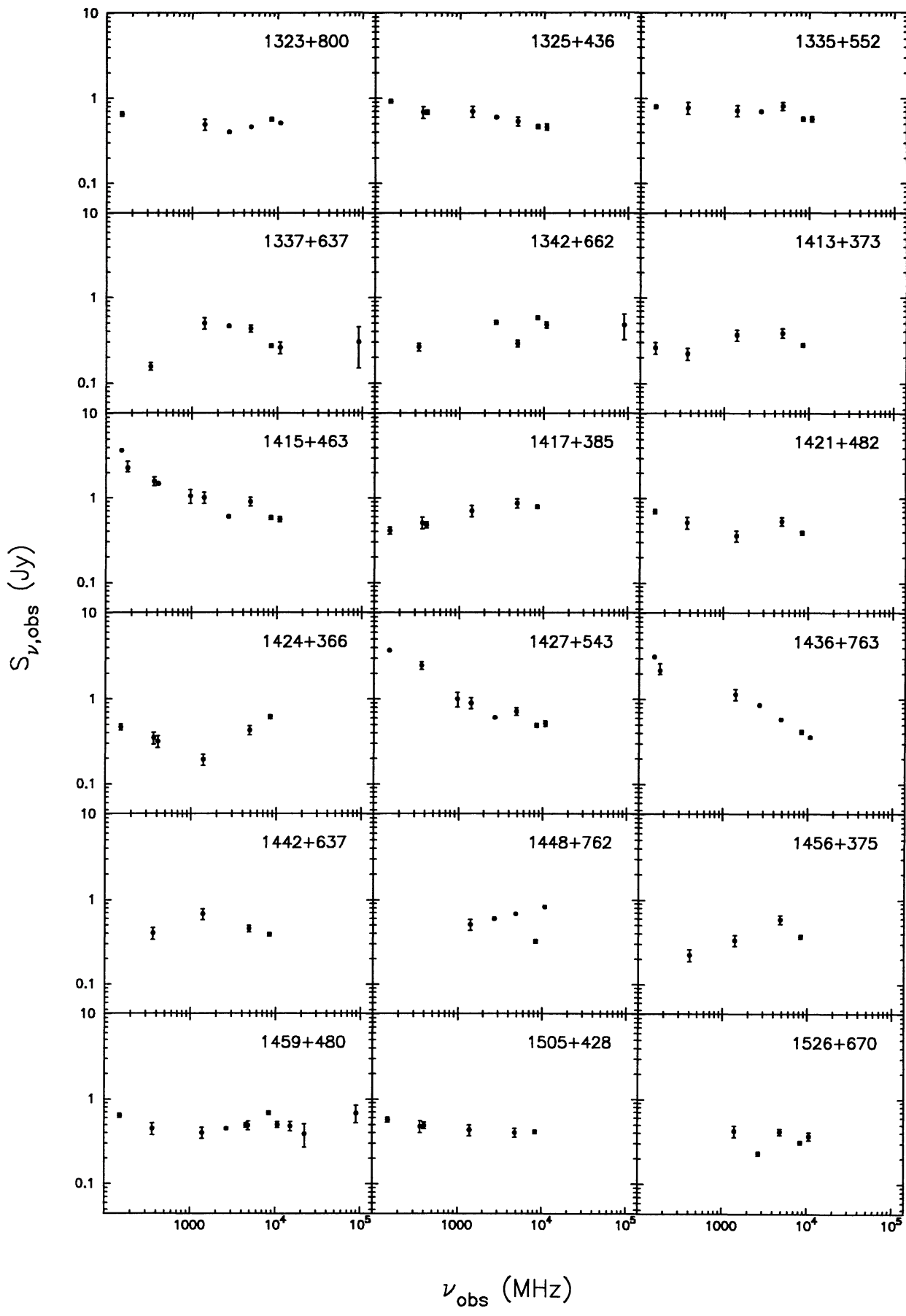


FIG. 3—Continued

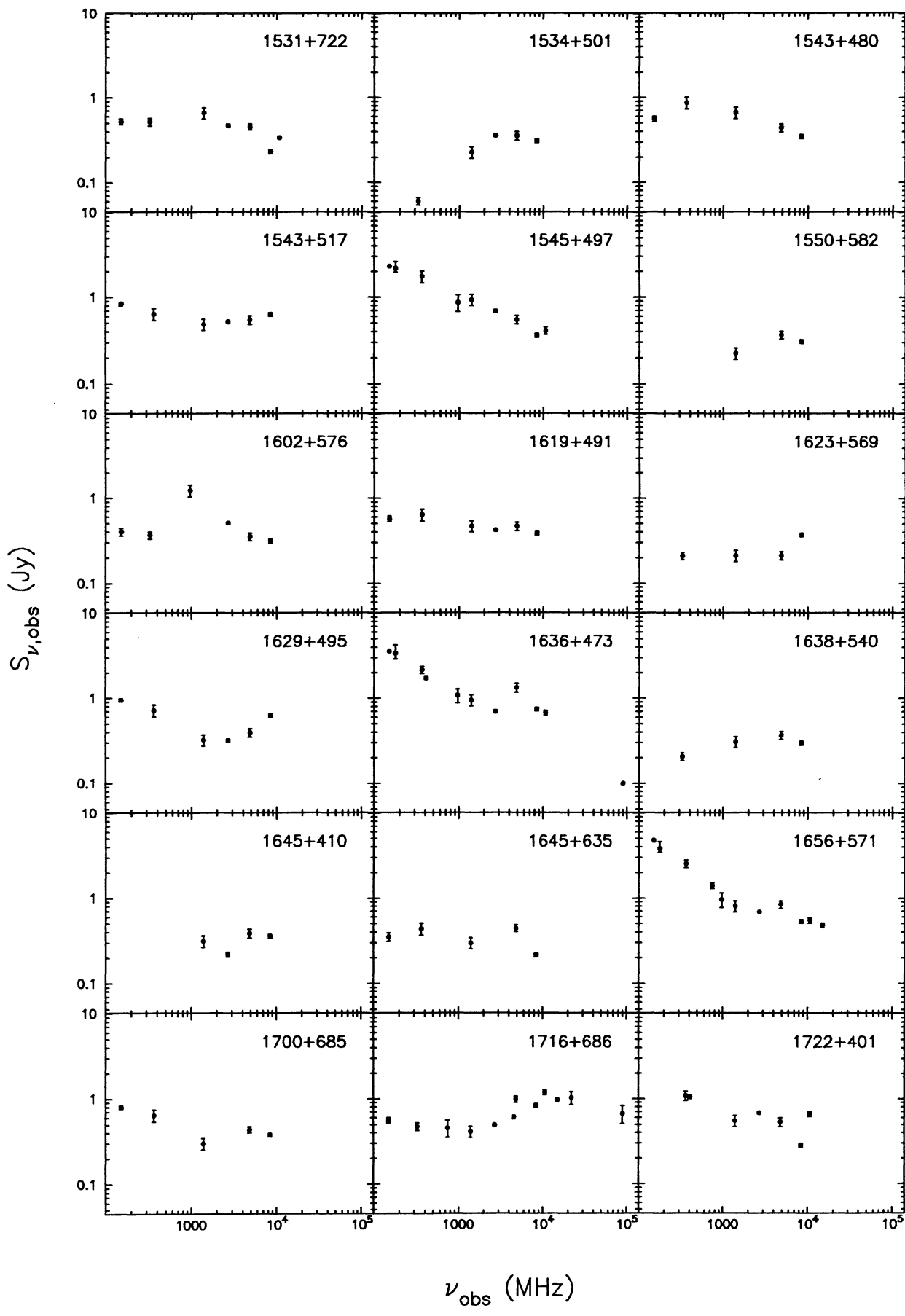


FIG. 3—Continued

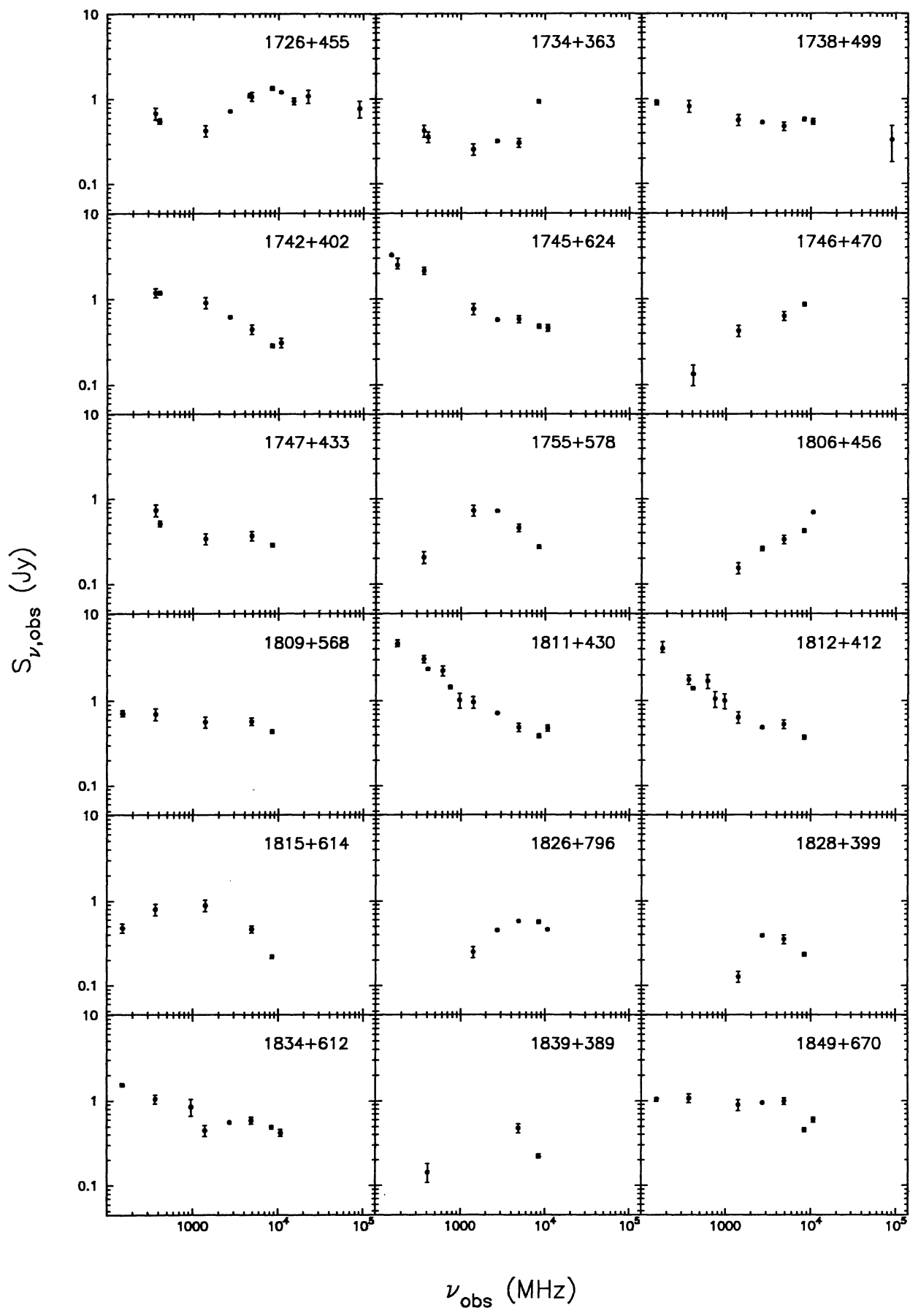


FIG. 3—Continued

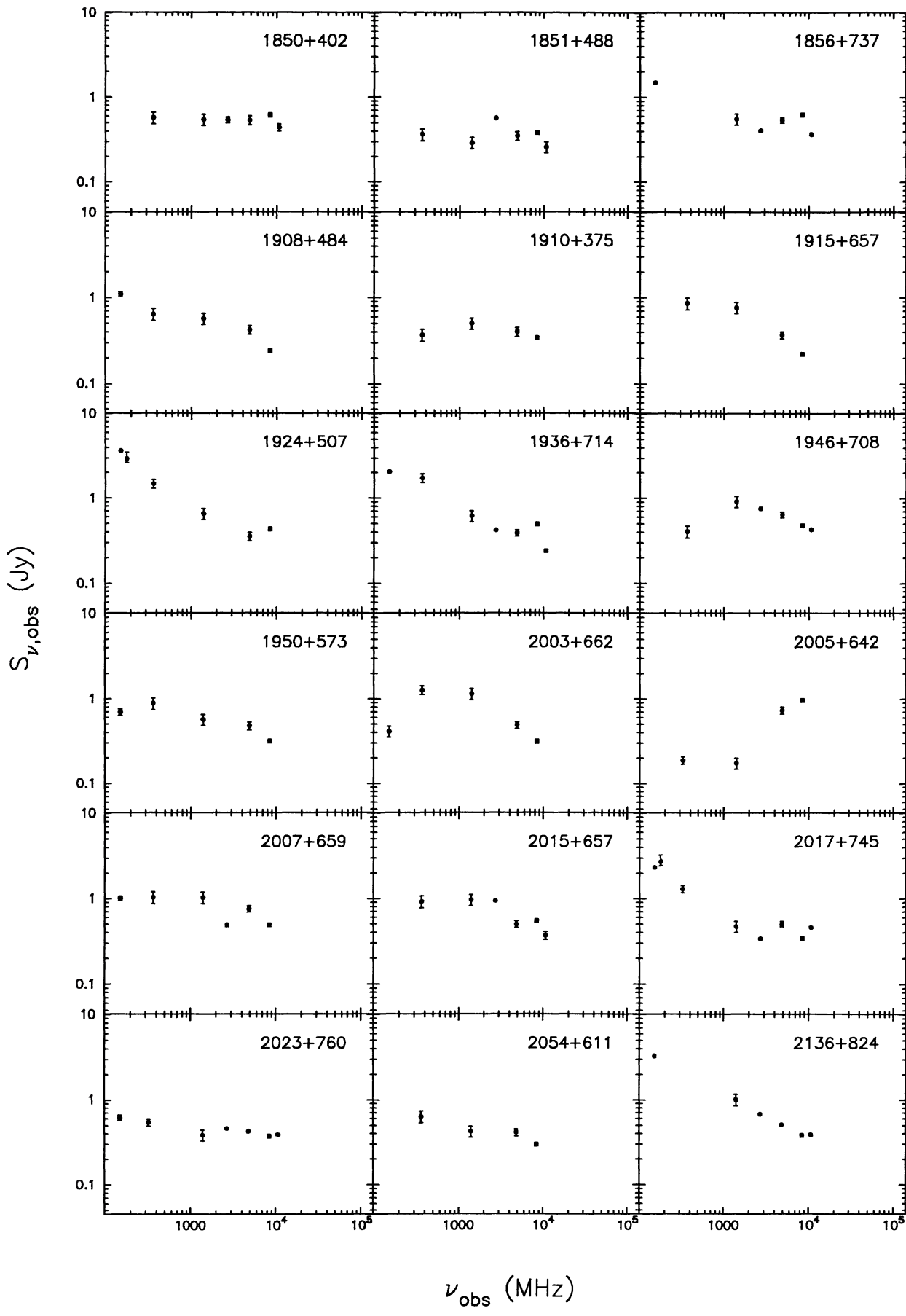


FIG. 3—Continued

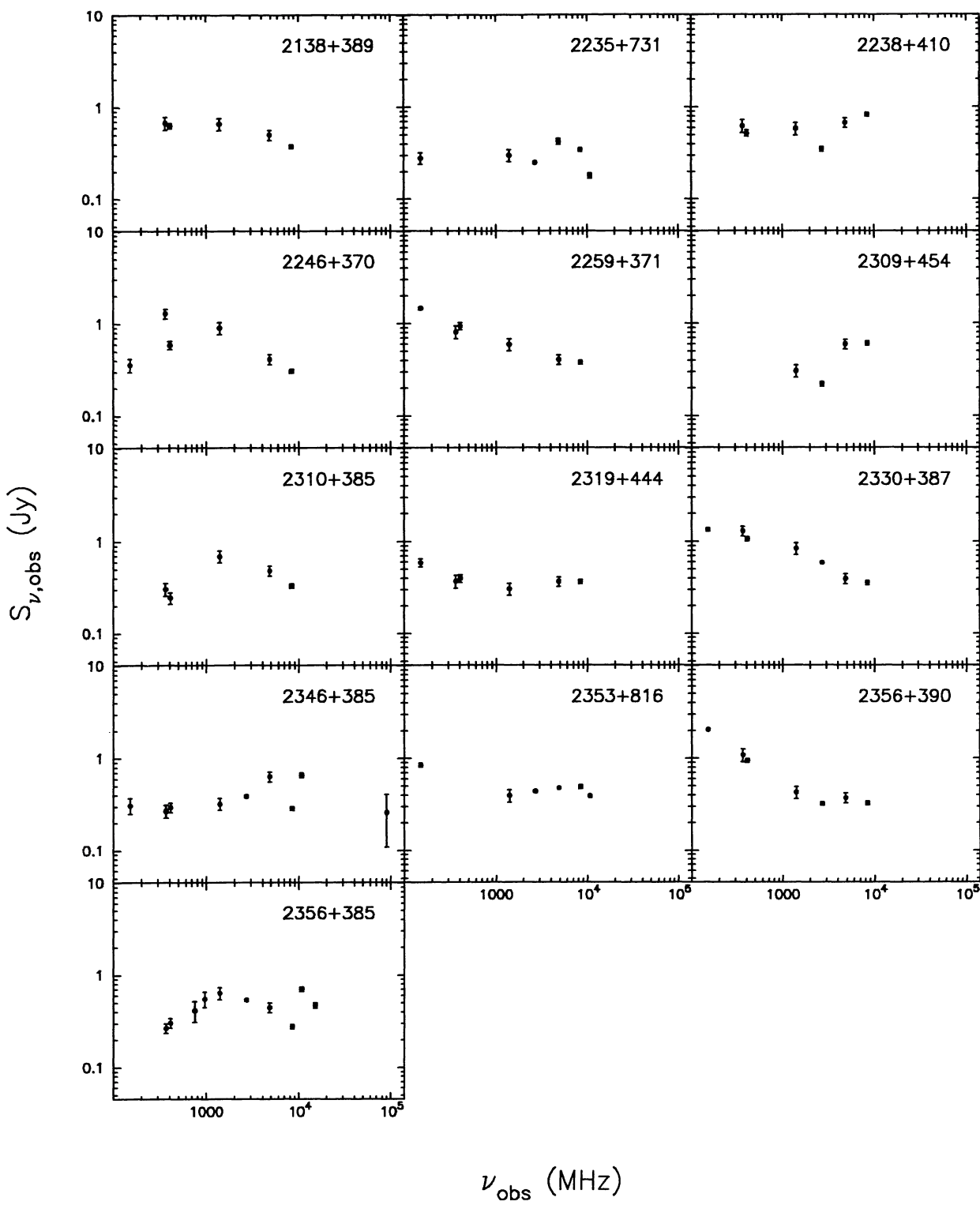


FIG. 3—Continued

TABLE 4
FLUX DENSITY CATALOGS

Frequency (MHz) (1)	Survey (2)	Reference(s) (3)	Typical Error (4)	Correction Factor (5)
151	6C	Baldwin et al. (1985), Hales, Baldwin & Warner (1988, 1993), Hales et al. (1990, 1991, 1993)	50 mJy	—
178	4C	Pilkington & Scott (1964), Gower, Scott & Wills (1967)	10%	1.09 ^a
318		Kühr et al. (1979)	150 mJy	—
327	WENSS	WENSS team, 1994, priv. comm.	10%	—
365	Texas	Douglas et al. (1980)	15 mJy	1.041 ^b
408	B2.3	Colla et al. (1973)	50 mJy	0.96 – 1.02 ^c
408	B3	Ficarra et al. (1985)	50 mJy	0.96 – 1.02 ^c
610	VRO	Macleod et al. (1965)	20%	1.065 ^d
750		Pauliny-Toth, Wade & Heeschen (1966)	200 mJy	1.059 ^e
750		Owen, Spangler & Cotton (1980)	100 mJy	1.035 ^e
966		Kühr et al. (1979)	—	—
968		Owen, Spangler & Cotton (1980)	100 mJy	1.026 ^e
1400		White & Becker (1992)	15%	—
2700		Kühr et al. (1979)	25 mJy	—
4585		Kühr et al. (1979)	40 mJy	—
4850	87GB	Gregory & Condon (1991)	15%	—
4890	S5	Kühr et al. (1981a)	5 mJy	—
8400	JVAS	Patnaik et al. (1992) and other JVAS papers in preparation	5%	—
10700		Kühr et al. (1979)	25 mJy	—
15000		Owen, Spangler & Cotton (1980)	40 mJy	—
15064		Kühr et al. (1979)	80 mJy	—
22185		Kühr et al. (1979)	150 mJy	—
31400		Kühr et al. (1979)	90 mJy	—
31400		Owen, Spangler & Cotton (1980)	200 mJy	—
90000		Kühr et al. (1979)	160 mJy	—
90000		Owen, Spangler & Cotton (1980)	200 mJy	—

NOTES.—Col. (1): The frequency of observation (in MHz). Col. (2): Name of the survey (if any); abbreviations are as follows: 6C, 6th Cambridge Survey; 4C, 4th Cambridge Survey; WENSS, Westerbork Northern Sky Survey; Texas, Texas Survey; B2.3, B3, Second Bologna Survey (Third Part) and Third Bologna Survey, respectively; VRO, Vermilion River Observatory Survey; 87GB, 1987 Green Bank Survey; S5, 5th Strong Source Survey; JVAS, Jodrell Bank – VLA Astrometric Survey. Col. (3): Reference(s) for the flux density catalog. A subsample of Kühr et al. 1979 containing only the sources stronger than 1 Jy at 5000 MHz was later published as Kühr et al. 1981b. Col. (4): Estimate of the typical uncertainty on the flux densities in the catalog, either in millijanskys or as a percentage of the flux density. Note that the error bars in Fig. 3 are taken predominantly from the uncertainties quoted for each flux density in the catalog, rather than these estimated values. Col. (5): The correction factor applied to the flux densities in the catalog to convert them to the absolute scale of Laing & Peacock 1980. Superscripts indicate source of correction factor: a, Roger, Bridle, & Costain 1973; b, J. Douglas, private communication; c, Riley 1988, correction factor depends on flux; d, Baars et al. 1977; e, Kühr et al. 1981b.

The flux density measurements for 1038+528 that were made with low-resolution instruments will be contaminated by a strong quasar, 1038+528B, located only 33" to the northwest. VLBI observations of both quasars are reported by Marcia & Shapiro (1984).

The spectral index distribution for the CJ2 sample is shown in Figure 4. Note that most flat-spectrum sources are variable, and since the flux density measurements at different frequencies were not simultaneous, the spectral indices derived are only representative and will differ from the instantaneous values. While the vast majority of the CJ2 sample have flat radio spectra, there are 13 “steep-spectrum” sources with $\alpha < -0.5$. Thus the CJ2 sample is not a perfect spectrally limited sample.

5. SUMMARY

Global VLBI images at 4992 MHz are presented for the 102 sources observed in the final observing session of the CJ2 survey. We also present integrated radio spectra for the entire CJ2 sample. Future papers will discuss the interpretation of these observations and of second-epoch observations. A concerted effort is underway to obtain redshifts for all objects in this sample.

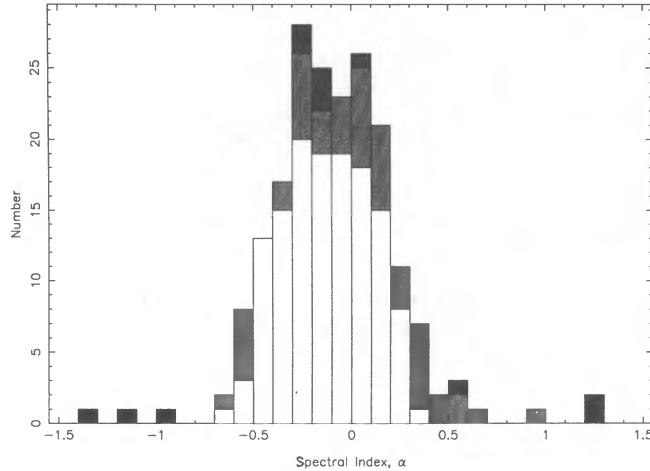


FIG. 4.—Distribution of spectral index (defined as $S_\nu \propto \nu^\alpha$) for the CJ2 sample. For most sources, α has been calculated between 365 MHz and 8400 MHz (shown with no shading). For 49 sources, with unknown 365 MHz flux densities, α has been calculated between 1400 MHz and 8400 MHz (gray shading); and for 12 sources, with both an unknown 365 MHz and 1400 MHz flux density, α has been calculated between 4850 MHz and 8400 MHz (black shading).

We thank the staff at the VLA, VLBA, and European VLBI Network observatories who took part in these observations and the staff of the JPL/Caltech Block II Correlator for their assistance. We also thank Sally Hales for help in obtaining the 151 MHz flux densities and for advice on the use of flux density scales. We are grateful to Jim Douglas for providing 365 MHz flux densities prior to publication and to Ger de Bruyn for providing 327 MHz flux densities from the WENSS prior to publication. We are indebted to Martin Shepherd for writing and maintaining DIFMAP and for the many modifications he made on our behalf. Thanks also to Roddy Calder for help with Figure 4. D. R. H. acknowledges the receipt of a SERC research studentship. The work done by the Caltech group was supported by the NSF under grant AST-9117100.

APPENDIX AGREEMENT FACTORS

Table 3 lists *agreement factors* between the models and observed visibilities. Separate agreement factors are given for amplitude and closure phase. In addition a total agreement factor (a weighted average of the amplitude and closure-phase agreement factors) is given; this is the quantity that is minimized in the least-squares model-fitting procedure. The closure-phase agreement factor is useful because it is not affected by antenna phase calibration errors.

A1. AMPLITUDE AGREEMENT FACTOR

Denoting the model amplitude and phase at a sample point by A_m and ϕ_m and the observed amplitude and phase by A_0 and ϕ_0 with standard errors σ_A and σ_ϕ , the *amplitude agreement factor* is

$$Q_{\text{AMP}} = \sqrt{\frac{1}{M} \sum_1^M \left(\frac{A_0 - A_m}{\sigma_A} \right)^2}, \quad (1)$$

where the sum is over M measured visibility samples. Assuming that all the samples are independent and that the measured amplitudes have a Gaussian distribution (high-SNR approximation), the sum of squares in this expression is distributed as χ^2 with M degrees of freedom, and Q_{AMP}^2 is a reduced χ^2 with expected value 1. (For a large number of degrees of freedom ν , the distribution of χ^2 is approximately normal with mean ν and standard deviation $\sqrt{2\nu}$.)

In the process of model fitting, a number m of parameters of the model are estimated from the data. This reduces the number of degrees of freedom from M to $M - m$, so the amplitude agreement factor, as defined above, is not strictly a reduced χ^2 . For Gaussian model fitting, m is usually small compared with M , so this distinction can be ignored, but for a clean-component model with hundreds of parameters (component flux densities and positions), m may be large, and the expected value of the agreement factor may be significantly less than 1.

When the data are self-calibrated, additional parameters (unknown antenna gains) are estimated from the data, so the number of degrees of freedom is reduced. For example, if the data are taken on an array of N antennas and $N(N - 1)/2$ baselines and if independent gains are estimated for each antenna for each integration, the number of degrees of freedom is reduced by a factor $(N - 3)/(N - 1)$, and the expected value of Q_{AMP} is $\sqrt{(N - 3)/(N - 1)}$ (e.g., 0.58 for $N = 4$ and 0.88 for $N = 10$). Wieringa (1992) has shown that for self-calibration with a perfect model, the noise in the visibility amplitudes after application of (noisy) gain solutions is *lower* than the noise in the input visibilities by a factor $\approx \sqrt{(N - 3)/(N - 1)}$. This leads to the reduction in the expected value of Q_{AMP} shown above.

A2. CLOSURE-PHASE AGREEMENT FACTOR

Closure phase is the sum of visibility phases around a triangle of baselines; e.g., for three antennas i, j, k ,

$$\psi_0^{(ijk)} = \phi_0^{(ij)} + \phi_0^{(jk)} - \phi_0^{(ik)}. \quad (2)$$

In the high-SNR approximation, the variance of the closure phase is given by

$$(\sigma_{\psi}^{(ijk)})^2 = (\sigma_{\phi}^{(ij)})^2 + (\sigma_{\phi}^{(jk)})^2 + (\sigma_{\phi}^{(ik)})^2. \quad (3)$$

In an array of N antennas in which all baselines are measured, there are $N(N - 1)/2$ visibility phase measurements from which $N(N - 1)(N - 2)/6$ closure phases can be formed. However, only $(N - 1)(N - 2)/2$ of these are independent.

The *closure-phase agreement factor* is defined in a similar way to the amplitude agreement factor but allows for the fact that the closure phases are not all independent:

$$Q_{\text{CLP}} = \sqrt{\frac{\sum_1^{M_{\text{CLP}}} f \left(\frac{\psi_0 - \psi_m}{\sigma_{\psi}} \right)^2}{\sum_1^{M_{\text{CLP}}} f}}, \quad (4)$$

where the sum is taken over all M_{CLP} available closure-phase samples, but the denominator $\sum f$ is now the number of independent closure phases, and the factor f is computed for each sampling interval as the number of independent closure phases divided by the total number of closure phases in that interval. If all baselines were observed, then $f = 3/N$.

REFERENCES

- Baars, J. W. M., Genzel, R., Pauliny-Toth, I. I. K., & Witzel, A. 1977, *A&A*, 61, 99
 Baldwin, J. E., Boysen, R. C., Hales, S. E. G., Jennings, J. E., Waggett, P. C., Warner, P. J., & Wilson, D. M. A. 1985, *MNRAS*, 217, 717
 Colla, G., et al. 1973, *A&AS*, 11, 291
 Douglas, J. N., Bash, F. N., Torrence, G. W., & Wolfe, C. 1980, *Univ. Texas Publ. Astron.*, 17
 Fircarra, A., Grueff, G., & Tomassetti, G. 1985, *A&AS*, 59, 255
 Gower, J. F. R., Scott, P. F., & Wills, D. 1967, *MmRAS*, 71, 49
 Gregory, P. C., & Condon, J. J. 1991, *ApJS*, 75, 1011
 Hales, S. E. G., Baldwin, J. E., & Warner, P. J. 1988, *MNRAS*, 234, 919
 ———. 1993, *MNRAS*, 263, 25
 Hales, S. E. G., Masson, C. R., Warner, P. J., & Baldwin, J. E. 1990, *MNRAS*, 246, 256
 Hales, S. E. G., Masson, C. R., Warner, P. J., Baldwin, J. E., & Green, D. A. 1993, *MNRAS*, 262, 1057
 Hales, S. E. G., Mayer, C. J., Warner, P. J., & Baldwin, J. E. 1991, *MNRAS*, 251, 46
 Kühr, H., Nauber, U., Pauliny-Toth, I. I. K., & Witzel, A. 1979, MPIfR preprint, 55
 Kühr, H., Pauliny-Toth, I. I. K., Witzel, A., & Schmidt, J. 1981a, *AJ*, 86, 854
 Kühr, H., Witzel, A., Pauliny-Toth, I. I. K., & Nauber, U. 1981b, *A&AS*, 45, 367
 Laing, R. A., & Peacock, J. A. 1980, *MNRAS*, 190, 903 (LP)
 MacLeod, J. M., Swenson, G. W., Jr., Yang, K. S., & Dickel, J. R. 1965, *AJ*, 70, 756
 Marcaide, J. M., & Shapiro, I. I. 1984, *ApJ*, 276, 56
 Napier, P. J., Bagri, D. S., Clark, B. G., Rogers, A. E. E., Romney, J. D., Thompson, A. R., & Walker, R. C. 1994, *Proc. IEEE*, 82, 658
 Owen, F. N., Spangler, S. R., & Cotton, W. D. 1980, *AJ*, 85, 351
 Patnaik, A. R., Browne, I. W. A., Wilkinson, P. N., & Wrobel, J. M. 1992, *MNRAS*, 254, 655
 Pauliny-Toth, I. I. K., Wade, C. M., & Heeschen, D. S. 1966, *ApJS*, 13, 65
 Pearson, T. J., & Readhead, A. C. S. 1988, *ApJ*, 328, 114 (PR)
 Pilkington, J. D. H., & Scott, P. F. 1964, *MmRAS*, 69, 183
 Polatidis, A. G., Wilkinson, P. N., Xu, W., Readhead, A. C. S., Pearson, T. J., Taylor, G. B., & Vermeulen, R. C. 1995, *ApJS*, 98, 1
 Riley, J. M. 1988, *MNRAS*, 233, 225
 Roger, R. S., Bridle, A. H., & Costain, C. H. 1973, *AJ*, 78, 1030
 Shepherd, M. C., Pearson, T. J., & Taylor, G. B. 1994, *BAAS*, 26, 987
 Taylor, G. B., Vermeulen, R. C., Pearson, T. J., Readhead, A. C. S., Henstock, D. R., Browne, I. W. A., & Wilkinson, P. N. 1994, *ApJS*, 95, 345 (Paper I)
 Thakkar, D. D., Xu, W., Readhead, A. C. S., Pearson, T. J., Taylor, G. B., Vermeulen, R. C., Polatidis, A. G., & Wilkinson, P. N. 1995, *ApJS*, 98, 33
 Vermeulen, R. C., & Taylor, G. B. 1995, *AJ*, 109, 1983
 Wieringa, M. H. 1992, *Exp. Astron.*, 2, 203
 White, R. L., & Becker, R. H. 1992, *ApJS*, 79, 331
 Xu, W., Readhead, A. C. S., Pearson, T. J., Polatidis, A. G., & Wilkinson, P. N. 1995, *ApJS*, 99, 297